FORESTRY AND NATURAL SCIENCES

Igor Sidorov

Applications of Dynamic Speckles in Optical Sensing

Publications of the University of Eastern Finland
Dissertations in Forestry and Natural Sciences

UNIVERSITY OF EASTERN FINLAND

IGOR SIDOROV

Applications of Dynamic Speckles in Optical Sensing

Publications of the University of Eastern Finland
Dissertations in Forestry and Natural Sciences
№ 120

Academic Dissertation
To be presented by permission of the Faculty of Science and Forestry for public examination in the Auditorium ML1 in Medistudia Building at the University of Eastern Finland, Kuopio, on September, 27, 2013, at 2 p.m.

Department of Applied Physics

Kopijyvä
Kuopio, 2013
Editors: Prof. Pertti Pasanen, Prof. Pekka Kilpeläinen, Prof. Kai Peiponen,
Prof. Matti Vornanen.

Distribution:
Eastern Finland University Library / Sales of publications
P.O. Box 107, FI-80101 Joensuu, Finland
tel. +358-50-3058396
julkaisumyynti@uef.fi
http:// www.uef.fi/kirjasto

ISBN: 978-952-61-1220-6 (printed)
ISSNL: 1798-5668
ISSN: 1798-5668
ISBN: 978-952-61-1221-3 (PDF)
ISSN: 1798-5676

Author's address: University of Eastern Finland
Department of Applied Physics
P.O. Box 1627
70211 KUOPIO
FINLAND
Email: igor.sidorov@uef.fi

Supervisors: Professor Alexei A. Kamshilin, Ph.D.
University of Eastern Finland
Department of Applied Physics
P.O. Box 1627
70211 KUOPIO
FINLAND
Email: alexei.kamshilin@uef.fi

Serguei S. Miridonov, Ph.D.
CICESE
Optics Department
Carretera Ensenada-Tijuana 3918
C.P. 22860 ENSENADA, B.C.
MÉXICO
Email: mirsev@cicese.mx

Reviewers: Professor Andrey A. Lipovskii, Ph.D.
St.-Petersburg State Polytechnic University
Department of Physics and Technology of Nanostructures
Polytechnicheskaja 29
195251 ST.-PETERSBURG
RUSSIA
Email: lipovskii@mail.ru

Adjunct Professor Jukka Räty, Ph.D.
University of Oulu
Unit of Measurement Technology, Cemis-Oulu
P.O. Box 51
87101 KAJAANI
FINLAND
Email: jukka.raty@oulu.fi

Opponent: Professor Steen G. Hanson, Ph.D.
Technical University of Denmark
Department of Photonics Engineering
DTU Risø Campus, OPL-128, Box 49
DK 4000 ROSKILDE
DENMARK
Email: vsgh@fotonik.dtu.dk

ABSTRACT

Laser speckle effect is in a sense unique. One part of the optical society working with coherent illumination considers it as a nuisance. So, in holography, laser interferometry, optical coherence tomography, laser-based information visualization, and many other fields the speckle effect is nothing but a noise. At the same time, another part of the society considers it as an asset, since the speckle effect provides ample opportunities for monitoring of displacements, deformations, and alterations of other properties of various objects. And even though the speckle effect is known for several decades, the fields related to it are still developing actively.

In this thesis, least detectable speckle transition equal to the average speckle size has been used as a criterion for estimation of the accuracy limits of the measuring systems based on the spatial filtration of dynamic speckles. It is shown that the resolution of any measuring system using the spatial filtration of dynamic speckles is defined only by the geometry of the optical system. Theoretical analysis of statistical properties of the signal in the systems with spatial filtering shows that the signal frequency can be evaluated with precision sufficient to achieve the highest possible accuracy. The developed theory allows for designing an optimal measuring system, and can be used for comparison of this system performance with that of the competing methods.

Also here has been proposed novel architecture of the scanning dynamic-speckles range sensor with a micro-electromechanical system (MEMS) deflecting mirror for surface scanning. Usage of the MEMS deflector makes the range sensor more compact, reliable and cost-efficient in comparison with the previously reported versions. It is shown that harmonic oscillations of the MEMS mirror do not compromise the sensor accuracy. For the signal processing here was used the zero-crossing method, which is simple, fast and robust.

The scheme typical for the dynamic-speckles range sensor has been used to demonstrate feasibility of new for detection of

the small defects on the surface of nontransparent scattering materials. This technique is immune to the low frequency optical noise and provides high fidelity of measurements. It is shown that its resolution is defined solely by the geometrical parameters of the optical system. Simplicity and versatility of the proposed technique provides a good basis for practical applications in the industrial quality inspection systems.

The novel method for estimation of light penetration depth (LPD) in turbid media which is also presented in this work is based on analysis of the spatial structure variations of the laser speckle patterns caused by the change of the illumination conditions. Simple theoretical model based on the theory of Bragg diffraction from volume holograms was used for description of the speckle patterns behavior. It is shown that this model allows quantitative estimation of the LPD if the refractive index of studied material is known, while qualitative LPD estimation does not require knowledge of any optical properties of the material.

Universal Decimal Classification: 531.715, 531.719.2, 535.374, 621.375.826, 681.586.5

INSPEC Thesaurus: optical sensors; lasers; measurement by laser beam; speckle; spatial filters; distance measurement; micromechanical devices; mirrors; surface measurement; light scattering; absorbing media; turbidity; quality control; inspection

Yleinen suomalainen asiasanasto: optiset anturit; lasersäteily; laserit; mikromekaniikka; etäisyydenmittaus; optiset ominaisuudet; pinnat; sameus; laadunvalvonta

Preface

The studies described in this thesis were carried out during the years 2008-2013 in the Department of Applied Physics, University of Eastern Finland. I wish to use this opportunity to thank all those who have contributed to my studies and supported my work toward this thesis during these five years. In particular, I wish to express my gratitude to the following persons.

First of all, I want express my deepest thanks to my principal supervisor Professor Alexei A. Kamshilin, Ph.D., for providing me opportunity to work as a part of his research group. I am grateful for inspiration, support and patient guidance that I received from him during my studies. I truly admire his experience, determination and dedication to work. I would also like to address profound gratitude to my other supervisor, Serguei S. Miridonov, Ph.D., for valuable guidance, fruitful discussions and many brilliant ideas.

I would like to give my thanks to Ervin Nippolainen for his valuable help, comments, suggestions, and both scientific and non-scientific discussions. I am grateful to current and former members of the Sensor Technology Group and stuff of the Department of Applied Physics for warm and pleasant working atmosphere. Additional thanks goes to Dmitry D. Semenov, Ph.D., for introducing me to dynamic speckles, Salvatore Di Girolamo, Ph.D., for good humor and valuable help, Laure Fauch, Ph.D., for long and interesting discussions, and Victor Teplov, M.Sc., for his support.

I offer my gratitude to the official reviewers Professor Andrey Lipovskii, Ph.D., and Adjunct Professor Jukka Räty, Ph.D., for their constructive criticism and valuable suggestions they served to improve this thesis.

I also thank my parents Nadezhda and Sergei for their love and support during my life, and my sister Irina for her encouragement and support during my studies. I also thank my friends

for their encouragements and support. My dearest thanks go to my wife Olesya for her endless love and support. Her care, support and patience made preparation of this thesis considerably easier. There are no words to describe how dear you are to me as a wife and mother of our son. I dedicate this thesis to my dearly loved Olesya and Daniil.

Finally, I acknowledge the Academy of Finland and the Finnish Funding Agency for Technology and Innovation (TEKES) for the financial support.

Kuopio, August 2013

Igor Sidorov

LIST OF ABBREVIATIONS

CCD	charge-coupled device
CMOS	complementary metal–oxide–semiconductor
2D	two-dimensional
SNR	signal-to-noise ratio
FFT	fast Fourier transform
MEMS	micro-electro-mechanical system
STFT	short-time Fourier transform
ZC	zero-crossing
RMS	root mean square
LPD	light penetration depth

LIST OF SYMBOLS

I	light intensity
$\mathbf{r}$	radius vector representing coordinate in the observation plane
$\mathbf{r}_0$	radius vector representing coordinate in the object plane
$G(\mathbf{r}, \mathbf{r}_0)$	correlation function of two speckle patterns
$g(\mathbf{r}, \tau)$	normalized space-time correlation function
r_S	average speckle size in the observation plane
w	beam radius on the object surface
A	scaling factor connecting relative beam-surface displacement and speckle pattern shift
l	distance between the object surface and the observation plane
R_W	wavefront curvature radius of the illuminating beam
ρ	distance from the beam waist to the surface
$\delta\lvert\mathbf{r}\rvert$	measurement uncertainty for speckle translation
$\delta\lvert\mathbf{r}_0\rvert$	measurement uncertainty for scaling factor
δA	measurement uncertainty for beam-surface shift
$\gamma_{\lvert\mathbf{r}0\rvert}$	relative error of beam-surface displacement estimation
γ_{A}	relative error of scaling factor estimation

$\delta\rho$	measurement error for distance between beam waist and surface
L	distance of speckle translation
δL	measurement uncertainty for speckle translation distance
r_T	speckle translation length
L_T	total speckle displacement
δL_T	measurement uncertainty for total speckle displacement
γ	relative measurement error
λ	wavelength of illuminating beam
NA	numerical aperture of illuminating beam
T	measurement time
V	relative surface velocity
δV	measurement error for relative surface velocity
V_S	speckle velocity
τ_{LT}	speckle lifetime
τ_C	coherence time of speckles
f_S	speckle bandwidth
f_0	central frequency of photodiode signal
Λ	period of spatial filter
f_D	half of photodiode signal bandwidth
τ_{CD}	correlation time of photodiode signal
D	aperture size of spatial filter
f	photodiode signal frequency
φ	photodiode signal phase
$\Delta\varphi$	phase difference between two signal samples
Δf	shift of signal frequency between two signal samples
$\sigma^2_{\Delta\phi}$	variance of random phase drift
$\sigma_{\Delta f}$	quadratic mean of frequency fluctuations
$\sigma_{\Delta f,T}$	frequency error accounting the averaging
γ_{SF}	relative accuracy for sensors with spatial filtering
ρ^*	distance between beam waist and surface for which condition $f_0=f_S$ is fulfilled
$\theta_D(t)$	deflection angle of MEMS scanning mirror
θ_{DF}	full (peak-to-peak) deflection angle of MEMS mirror
Ω	MEMS resonant frequency

R	distance from mirror to beam waist
$V_{FS}(t)$	velocity of beam waist
ρ_0	shortest distance between beam waist and surface
T_F	measurement window
T_W	signal segment
Δx	surface displacement necessary for formation of one period of photodiode signal modulation
M	scaling coefficient showing period of spatial filter expressed in average speckle sizes
E	light amplitude
Z	effective penetration depth
n	refractive index
K	hologram vector
θ	incidence angle in the air
θ_n	incidence angle in the medium
$\delta\theta$	change of incidence angle in the air due to object rotation
$\delta\theta_n$	change of incidence angle in the medium due to object rotation
ζ	mismatch parameter
C	maximum of correlation function
C_0	maximum of autocorrelation function
a,b,c,d	model parameters

LIST OF ORIGINAL PUBLICATIONS

This thesis is based on data presented in the following articles, referred to by the Roman numerals (I-VI).

I Miridonov S. V., Sidorov I. S., Nippolainen E., and Kamshilin A. A., "Accuracy of measuring systems using dynamic speckles," *Journal of the Optical Society of America A* **26**, 745–753 (2009).

II Sidorov I. S., Miridonov S. V., Nippolainen E., and Kamshilin A. A., "Distance sensing using dynamic speckles formed by micro-electro-mechanical-systems deflector," *Optical Review* **17**, 161–165 (2010).

III Sidorov I. S., Nippolainen E., and Kamshilin A. A., "Detection of small surface defects of nontransparent scattering materials by using dynamic speckles.," *Applied Optics* **51**, 1781–1787 (2012).

IV Semenov D. V., Sidorov I. S., Nippolainen E., and Kamshilin A. A., "Speckle-based sensor system for real-time distance and thickness monitoring of fast moving objects," *Measurement Science and Technology* **21**, 045304 (2010).

V Sidorov I. S., Miridonov S. V., Nippolainen E., and Kamshilin A. A., "Estimation of light penetration depth in turbid media using laser speckles.," *Optics Express* **20**, 13692–13701 (2012).

VI Sidorov I. S., Miridonov S. V., Nippolainen E., and Kamshilin A. A., "Light penetration depth of a turbid media estimated by cross-correlation of speckle patterns," *Proceedings of the SPIE* **8413**, 84130B-1–84130B-6 (2012).

LIST OF CONFERENCE PRESENTATIONS

The data discussed in this thesis were presented on following scientific conferences:

I **Oral presentation: "**Accuracy of speckle range sensing." Sidorov I. S., Semenov D. V., Nippolainen E. and Kamshiln A. A., *Optics Days 2008*, Kuopio, Finland, 08.05.2008 - 09.05.2008.

II **Invited presentation:** "Dynamic speckles for distance measurements: what is the accuracy limit?." Kamshilin A. A., Miridonov S. V., Sidorov I. S. and Nippolainen E., *The 4th Finish-Russian Photonics and Laser Symposium*, Tampere, Finland, 25.05.2009 - 25.05.2009.

III **Invited presentation:** "Distance measurements by using dynamic speckles." *International Conference "Micro- to Nano-Photonics - ROMOPTO 2009"*, Kamshilin A. A., Miridonov S. V., Sidorov I. S. and Nippolainen E., Sibiu, Romania, 31.08.2009 - 31.08.2009.

IV **Invited presentation:** "Distance sensing using dynamic speckles formed by MEMS deflector." Kamshilin A. A., Miridonov S. V., Sidorov I. S. and Nippolainen E., *Eight Japan-Finland Joint Symposium on Optics in Engineering*, Tokyo, Japan, 04.09.2009 - 04.09.2009.

V **Oral presentation:** "Accuracy limit of a dynamic-speckles based measuring system", Sidorov I. S. , Nippolainen E, Miridonov S. V. and Kamshilin A. A., *The Ninth International Conference on Correlation Optics*, Chernivtsi, Ukraine, 20.09.2009 - 24.09.2009.

VI **Poster presentation:** "Detection of small surface defects of large metallic sheets by using dynamic speckles."

Sidorov I. S. , Nippolainen E and Kamshilin A. A., *Optics Days 2011*, Oulu, Finland, 12.05.2011 - 13.05.2011.

VII **Poster presentation:** "Estimation of light penetration depth in turbid media using laser speckles." Sidorov I. S. , Miridonov S. V., Nippolainen E and Kamshilin A. A., *The 5th Finnish-Russian Photonics and Laser Symposium*, St.-Petersburg, Russian Federation, 18.10.2011 - 20.10.2011.

VIII **Oral presentation:** "Dynamic speckles for fast mapping of surface defects." Sidorov I. S. , Nippolainen E and Kamshilin A. A., *The 3rd International Topical Meeting on Optical Sensing and Artificial Vision*, St.-Petersburg, Russian Federation, 14.05.2012 - 17.05.2012.

IX **Poster presentation:** "Surface defect detection systems based on dynamic speckles." Sidorov I. S. , Nippolainen E and Kamshilin A. A.,*The 8th International Conference on Optics-Photonics Design and Fabrication*, St.-Petersburg, Russian Federation, 02.07.2012 - 05.07.2012.

X **Oral presentation:** "Light penetration depth of a turbid media estimated by cross-correlation of speckle patterns." Sidorov I. S. , Miridonov S. V., Nippolainen E and Kamshilin A. A., *Speckle 2012: V International Conference on Speckle Metrology*, Vigo, Spain, 10.09.2012 - 12.09.2012.

XI **Poster presentation:** "Detection of surface defects by means dynamic speckles." Nippolainen E, Sidorov I. S. and Kamshilin A. A., *Speckle 2012: V International Conference on Speckle Metrology*, Vigo, Spain, 10.09.2012 - 12.09.2012.

XII **Oral presentation:** "Light penetration depth of a turbid media estimated by cross-correlation of speckle patterns." Sidorov I. S. , Miridonov S. V., Nippolainen E and Kamshilin A. A., *Northern Optics 2012*, Snekkersten, Denmark, 19.11.2012 - 21.11.2012.

AUTHOR'S CONTRIBUTION

Publication I is dedicated to estimation of theoretical limits of the accuracy of measuring systems based on spatial filtration of dynamic speckles. Theoretical basis of the publication was developed by S. V. Miridonov. The author of this thesis was responsible for experimental verification of the theoretical predictions. Using advices of E. Nippolainen the author has designed and assembled the experimental setup and acquired the experimental data for the publication. The author also did preliminary data analysis, while final analysis was done by S. V. Miridonov. The publication was written by S. V. Miridonov and A. A. Kamshilin with minor comments from I. S. Sidorov and E. Nippolainen.

Publication II presents novel architecture of the diffraction range sensor. The idea to use MEMS scanning mirror as a deflector for generation of dynamic speckles belongs to A. A. Kamshilin. Theoretical justification of usage of the MEMS scanner for range sensing was given by S. V. Miridonov. The thesis author has designed the experimental setup and acquired the data, after receiving comments from S. V. Miridonov and E. Nippolainen. Analysis of the experimental data was done by S. V. Miridonov. The publication was prepared by I. S. Sidorov in close collaboration with S. V. Miridonov and A. A. Kamshilin.

Publication III demonstrates novel technique for detection of fine surface defects using spatially filtered dynamic speckles. The original idea belongs to A. A. Kamshilin and E. Nippolainen. The theoretical basis of the method was developed by A. A. Kamshilin with contribution from the author. The author with help of E. Nippolainen has designed the experimental setup used for verification of the method feasibility. Also, the author have designed and assembled the optical head of the diffraction defectoscope prototype, while its electronic part was designed by E. Nippolainen. Data processing algorithm and software for the prototype were developed by I. S. Sidorov and E. Nippolainen. The author was responsible for preparing the

results and wrote the article, after receiving comments from the co-authors.

Publication IV presents prototype of the scanning dynamic-speckles range sensor. The prototype was designed and assembled by D. V. Semenov and E. Nippolainen. The thesis author was responsible for preparation of the experimental results. The article was written by D. V. Semenov while receiving comments from the co-authors.

Publications V and VI are devoted to study of the optical penetration depth in turbid media using laser speckles. The original idea and theoretical basis of the method were developed by S. V. Miridonov. In both cases the author has designed the experimental setups using valuable comments from S. V. Miridonov and E. Nippolainen. Analysis of the experimental data was done by S. V. Miridonov and I. S. Sidorov. Both articles were written by the author after receiving comments from the co-authors.

Contents

1 Introduction

Invention of the light amplification by stimulated emission of radiation (LASER) in the early sixties of the previous century has provided unique possibilities for researchers and industry [1]. However, illumination of any optically rough surface with a coherent light source (even with a femtosecond lasers [2]) inevitably leads to irregular distribution of the scattered light intensity at the observation plane. This granular intensity distribution called "speckle pattern" is formed due to the interference of a large number of waves scattered by the surface irregularities [3]. Note that the surface can be considered optically rough when the surface irregularities are larger or comparable with the wavelength of the illumination. Initially the speckle effect was considered only as an optical noise affecting information content and resolution of the images. For that reason multiple techniques of speckle reduction were developed in such fields as holography [4–9], holographic interferometry [10], holographic microscopy [11], laser microscopy [12–14], optical coherence tomography [15–19], laser-based information visualization [20] and some others. A good review of the speckle reduction techniques is given in [21].

But in a little while it was found that the speckle effect can be used to monitor displacements and deformations of objects. Nowadays various methods and techniques based on the speckle effect are grouped under the name "Speckle metrology". Excellent survey of this field is given in the book of the same name edited by R. S. Sirohi [22]. The speckles can be used for analysis of behavior of a car parts [23], monitoring of a paint drying process [24], study of a metal [25,26] or stone corrosion [27], image reconstruction [28,29], displacement sensors [30] and blood flow measurements [31] to name but a few applications.

The majority of the measurement methods based on the speckle effect are dealing not with the static speckle patterns,

but with the ones varying along with the changes of the object properties. Such time-varying speckles are traditionally referred to as "dynamic". Although dynamic speckles are known for many decades it would not be wrong to say that both their study and list of their applications are yet to be completed. For instance, the classical study of accuracy of measuring systems using spatial filtering of dynamic speckles performed by Veselov and Popov [32] does not take into account averaging process during long-term measurements. This incompleteness of the accuracy study hamper comparison of characteristics of these measuring systems with that of the systems based on alternative methods. Therefore, the study of measuring accuracy of the systems using spatial filtering should be supplemented. In their turn, characteristics of the scanning dynamic speckles range sensors [33–35], which can be used as a good example of measuring systems based on dynamic speckles, in addition to other factors are defined by the properties of the deflector used in the optical setup. Thus, proper choice of the deflector can both improve performance of the range sensor and make the sensor more attractive for industrial applications. Moreover, there is always need for new simple and cost-effective optical systems suitable for fast sensing and monitoring of various physicotechnical parameters in industrially oriented tasks. The dynamic speckle effect is a good basis for development of such optical sensors.

The aim of this work is to address problems indicated in the previous paragraph. Theoretical limits of achievable accuracy for measuring systems based on spatial filtration of the dynamic speckles will be discussed in Chapter 2. Novel architecture of the dynamic speckles range sensor will be presented in Chapter 3. Finally, original technique and system for detection of small surface defects based on the analysis of spatially filtered dynamic speckles and novel method for experimental estimation of the light penetration depth in turbid media utilizing the analysis of structural changes of speckle patterns caused by variation of the illumination angle will be introduced and discussed in Chapter 4 and Chapter 5, respectively.

2 Accuracy of sensors based on spatial filtration of dynamic speckles

As it was mentioned in the introduction, the speckle pattern is observed when the coherent laser beam illuminates optically rough surface. Already in the in the first works reporting discovery of the speckle effect [36–38] it was noted that when the beam and the surface are displacing in respect to each other the speckle pattern changes in both time and space, or in other words it becomes dynamic. There are two types of the speckle dynamics: translation and boiling [39]. The former denotes shifting of the whole speckle pattern with its spatial structure remaining almost constant in response to the relative beam-surface displacement. The later stands for such changes of the speckle pattern when every single speckle is changing its shape, size and position individually while the whole pattern does not move. Since pure types of the speckle dynamics are rarely observed, in the majority of cases those types are combined. It means that usually translational motion of the speckle pattern is accompanied by the shape deformation of individual speckles. Rate of the speckle shape changes is defined by the proportion between speckle translation and boiling, which in its turn depends on the optical configuration used for observation of the dynamic speckles. When the illumination is done by a divergent Gaussian beam and the speckles are observed after the free space propagation of the scattered light the translation dynamic of speckles is always prevailing over the boiling if the illuminated surface is situated outside of the beams Rayleigh range and the distance from the beam waist to the surface is smaller than that between the surface and the observation plane [40].

The fact that the motion of dynamic speckles is defined by the configuration of the optical system and the relative velocity of the surface from which the light was scattered [41–47] can be used in ether velocity [45,46] or range [48,49] sensing. In both cases unknown quantity is estimated through the measurement of the dynamic speckle pattern velocity, i.e. its displacement within specified time interval. One of the methods which is widely used for estimation of the speckle pattern changes was proposed by Yamaguchi [50] and was later supplemented by works of Sjödahl [51] and Horváth et al. [52]. This method, currently known as electronic (digital) speckle photography, is based on the correlation of the speckle patterns generated by the object under investigation and recorded using matrix photodetector arrays (CCD or CMOS) during object's deformation (translation, rotation, etc.). Judging from the behavior of the correlation peak one can estimate the nature and magnitude of the deformation. In our case, displacement of the speckle pattern is estimated from the position of the correlation peak. Accuracy of this method is defined by a number of parameters of the measuring system, i.e. image sensor noise level, average speckle size in pixels, total amount of pixels and some other. When these parameters are optimized and proper image processing algorithm is used, this method can yield the accuracy comparable or even equal to the Cramér-Rao bound. However, at the high object velocity other system properties, namely sensor frame rate and the data processing speed, become critical. In particular, when the object velocity exceeds several meters per second the requirements to the sensor frame rate and data processing speed become either very tough, or completely unreasonable.

Another method for estimation of the speckle pattern velocity is based on the spatial filtration. This method was proposed by Ator for estimation of movement velocity at aerial survey [41]. Later he has developed the theoretical basis of this method in [44]. Spatial filtration of the moving image by the diffraction grating or by the binary filter consisting of the stopping and transmitting stripes allows for estimation of the image velocity. The velocity is estimated from the signal of a single

photodetector situated after the filter. Therefore, amount of data required for velocity estimation is reduced dramatically and speed of the object movement is not the limiting factor. Stavis was the first one to apply the spatial filtration to the dynamic speckle patterns [46]. At the moment, spatial filtration is the simplest method for estimation of the dynamic speckle velocity. As it was mentioned before, the dynamic speckles can be used in velocity and range sensors. However, the speckles are stochastic in nature, which implies certain restrictions on the accuracy of the measurements. Whereas accuracy of the commonly used methods, such as triangulation or time-of-flight for distance measurements, was thoroughly studied (e.g., see review of laser ranging techniques given by Amann et al. in [53]), there were no comprehensive theoretical estimations of achievable accuracy of measuring instruments using spatially filtered dynamic speckles. Without these estimations one can neither find the best design of a measuring system providing the highest measurement accuracy for a specific application, nor adequately compare performance of that system with that of another systems. Original theoretical estimation of accuracy limits of the measuring systems utilizing spatial filtration of the dynamic speckles will be presented in this chapter.

2.1 RELATIVE ACCURACY OF MEASUREMENTS

As one already knows, the spatial filtration of the dynamic speckles is mainly used in diffraction velocimeters and range sensors. In the velocimeters and early versions of the range sensors dynamic speckles are typically originate from the movement of an optically rough surface or a particle flow in respect to the fixed laser beam, as shown in Fig. 2.1(a). The situation typical to the recent modifications of range sensors, where dynamic speckles are formed by the rapid scan of the fixed or slowly moving surface with a deflected laser beam, is illustrated in Fig. 2.1(b).

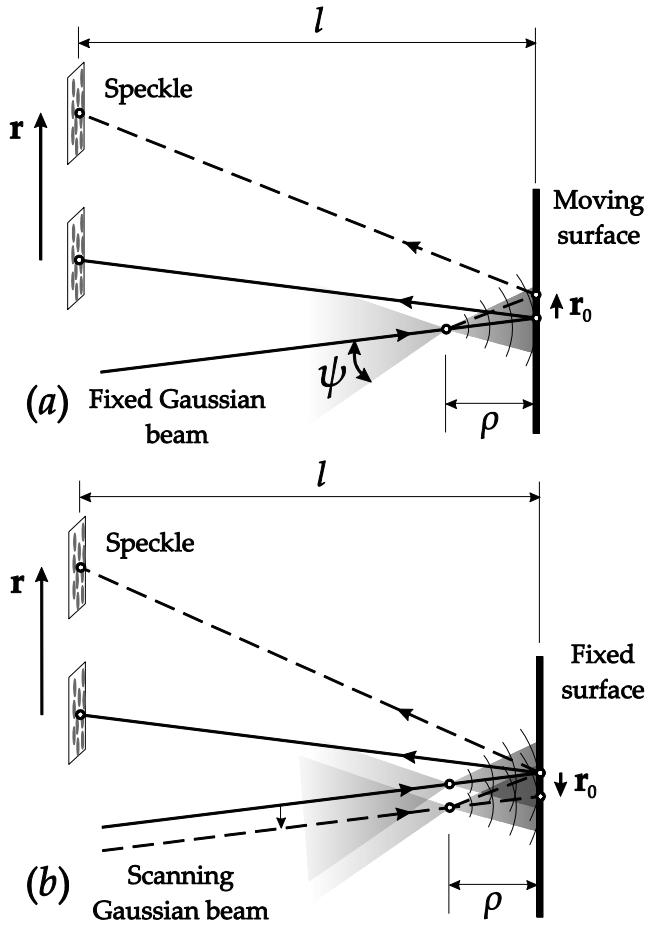

Figure 2.1 *Two configurations for the formation of dynamic speckles: (a) moving object and (b) scanning laser beam. (Originally from* ***Paper I****)*

In the observation plane translating speckle pattern can be presented as a two-dimensional (2D) intensity distribution $I(\mathbf{r}',\mathbf{r}_0)$, where $\mathbf{r}$ is the radius vector representing the coordinate and $\mathbf{r}_0$ is a vector parameter related to the surface plane representing the shift of the laser beam in respect to the object surface. The speckles dynamics can be described by a 2D correlation function, which is evaluated as integration over the speckle pattern area ($\mathbf{r}' \in S$), of two speckle patterns obtained for different relative beam-surface positions:

$$G(\mathbf{r},\mathbf{r}_0) = \int_S I(\mathbf{r}'-\mathbf{r},\mathbf{r}_0) I(\mathbf{r}',\mathbf{r}_0)\mathrm{d}S\,. \tag{2.1}$$

Normalized space-time correlation functions of the speckle patterns $g(\mathbf{r},\tau) = G(\mathbf{r},\tau)/\overline{G}(\mathbf{r},\tau)$ with removed mean value calculated for the most of illumination and observation conditions were presented in [54]. And for the case when the object illumination is done by a Gaussian beam and the scattered light is observed after a free space propagation the correlation function, with a slight modification described in [55], can be written in only spatial representation as

$$g(\mathbf{r},\mathbf{r}_0) - 1 = \exp\left(-\frac{\left|\mathbf{r} - A\mathbf{r}_0\right|^2}{r_S^2}\right)\exp\left(-\frac{\left|\mathbf{r}_0\right|^2}{w^2}\right). \qquad (2.2)$$

Here r_S is the average speckle size in the observation plane, w is the beam radius on the object surface, and A is a scaling factor connecting relative beam-surface displacement with the shift of the speckle pattern in the observation plane. Analysis of the first exponential term in Eq. (2.2) shows that correlation function has a maximum at the condition $\mathbf{r} = A\mathbf{r}_0$, which means that relative beam-surface displacement by $\mathbf{r}_0$ corresponds to the shift of the spackle pattern by $A\mathbf{r}_0$.

The scaling factor can be presented in the terms of geometrical parameters of the optical setup: distance between the object surface and the observation plane l, and the wavefront-curvature radius of the illuminating beam R_W. It should be noted that the scaling factor is different for the cases illustrated in Fig. 2.1. In the first case, which was thoroughly studied in the second half of last century [56–60], the moving surface is illuminated by the fixed laser beam [Fig. 2.1(a)] and the scaling factor has a form $A^{(a)} = 1 + l/R_W$. In the second case, interest to which has appeared only recently [33], the deflecting laser beam rapidly scans the fixed or slowly moving surface and the scaling factor can be represented as $A^{(b)} = l/R_W$ [55]. Since, as it was mentioned above, when the illumination is done by a divergent Gaussian beam and the object is situated outside of the Rayleigh range of the beam the translation dynamic of speckles is always prevailing, only that illumination type will be considered in this work. Usually the distance from the beam waist to the surface ρ (see

Fig. 2.1) is much larger that the Rayleigh range. In this case the beam wavefront-curvature radius can be assumed to be equal to this distance, $R_W \approx \rho$. It is also assumed here that $l >> \rho$, which is valid for the majority of the measuring systems.

Knowing the translation distance of the speckle pattern $\mathbf{r}$ and using relation $\mathbf{r} = A\mathbf{r}_0$ one can easily find ether the scaling factor A or the surface displacement $\mathbf{r}_0$. On the one hand, in velocimeters position of the optical head is fixed and consequently the scaling factor A is known. Therefore, knowledge of the speckle translation allows estimation of surface displacement $\mathbf{r}_0$, which is directly related to the surface speed. On the other hand, in range sensors the relative surface speed is known, which makes $\mathbf{r}_0$ known parameter. Consequently the speckle translation allows estimation of the coefficient A and, since usually value $(l - \rho)$ is known, the distance ρ.

Thereby, in both velocimeters and range sensors the speckle translation $\mathbf{r}$ is the key parameter for estimation of the measurand. Consequently, errors in evaluation of this parameter lead to uncertainties in the final results. From the theory of errors we know that errors in the relation $|\mathbf{r}| = A|\mathbf{r}_0|$ are connected as $(\delta|\mathbf{r}|)^2 = A^2(\delta|\mathbf{r}_0|)^2 + (\delta A)^2|\mathbf{r}_0|^2$, where $\delta|\mathbf{r}|$, δA and $\delta|\mathbf{r}_0|$ are measurement uncertainties for speckle translation, scaling factor and beam-surface shift, respectively. This equation can be used for calculation of relative errors for both velocimeters and the range sensors. As was mentioned above, in velocimeters the scaling factor A is known ($\delta A = 0$). In this case equation for the error in the estimation of the beam-surface displacement can be written as $\delta|\mathbf{r}_0| = \delta|\mathbf{r}|/A$. And this equation allows calculation of the relative error of beam-surface displacement as

$$\gamma_{|\mathbf{r}_0|} = \frac{\delta|\mathbf{r}_0|}{|\mathbf{r}_0|} = \frac{\delta|\mathbf{r}|}{|\mathbf{r}|}. \qquad (2.3)$$

It is easy to see that since in range sensors the relative surface velocity and consequently the surface displacement are known ($\delta\mathbf{r}_0 = 0$), the relative error of the scaling factor is also equal to the relative error of the speckle translation:

$$\gamma_A = \frac{\delta A}{A} = \frac{\delta|\mathbf{r}|}{|\mathbf{r}|}. \tag{2.4}$$

In its turn, the relative error in the evaluation of the scaling factor A defines the relative error in the estimation of distance ρ. Since in the most of arrangements $l >> \rho$, it is easy to show that

$$\left|\frac{\delta A}{A}\right| \approx \left|\frac{\delta\rho}{\rho}\right| \tag{2.5}$$

Therefore, calculation of the relative error of the speckle pattern translation provides estimation of relative errors for both types of measuring systems: velocimeters and range sensors.

2.2 DIFFRACTION-LIMITED ACCURACY

As it was shown, in the measuring systems based on the spatial filtration of dynamic speckles the measuring accuracy is defined by the errors in the estimation of the translation distance of the speckle patterns. These errors stem from the stochastic nature of speckles. The behavior of speckles is strongly dependent on the diffraction properties of light implied by the parameters of the Gaussian beam and features of the optical setup. It is only natural to consider these properties of light as a main factor limiting the accuracy in the discussed systems. In addition, here for simplicity reasons the laser power and an optical noise are excluded from consideration.

A standard method of evaluation of a speckle pattern translation is to calculate crosscorrelation function for two speckle pattern snapshots taken before and after the translation. The distance of the speckle translation, $|\mathbf{r}| = L$, is evaluated from the position of the correlation maximum. Since the light diffraction is chosen as the main factor limiting the accuracy, it is assumed here that estimation uncertainty in the translation measurements is equal to the correlation radius of speckle, $\delta|\mathbf{r}| = \delta L = r_S$. It is clear that the relative accuracy $\delta L/L$ improves with the in-

crease of the speckle translation distance L. However, analysis of Eq. (2.2) shows that magnitude of the correlation peak is inversely proportional to that distance. As the most reasonable speckle translation can be considered shift of the pattern that causes the decay of the correlation peak by e. It is clear from the second exponential term of the Eq. (2.2) that such speckle translation is equal to $r_T = A\,w$. The parameter r_T is called speckle translation length. Thereby, in a single measurement one can measure translation of speckles by r_T with the accuracy r_S. The measurement can be continued using the second snapshot as an original one and taking another snapshot after the speckle translation by r_T. In case when that operation is repeated N times the speckle pattern is translated by the distance $L_T = N r_T$. Supposing that errors in each measurement are random and independent the uncertainty of this measurement can be written as $\delta L_T = \sqrt{N} r_S = r_S \sqrt{L_T / r_T}$. Therefore, one can estimate the relative error of the whole measurement as:

$$\gamma = \frac{\delta L_T}{L_T} = \frac{r_S}{\sqrt{r_T L_T}} . \tag{2.6}$$

The total speckle displacement, L_T, corresponds to the surface displacement $L_S = L_T / A$. Taking into account that the speckle translation distance is defined as $r_T = A\,w$, the Eq. (2.6) can be rewritten as:

$$\gamma = \frac{r_S}{A\sqrt{w L_S}} . \tag{2.7}$$

In addition, the average speckle size is defined as $r_S = l\lambda/(\pi w)$, where λ is the wavelength of the illuminating beam. The beam radius at the object surface is expressed as $w = \rho\,\mathrm{NA}$, where $\mathrm{NA} = \sin(\psi)$ [see Fig. 2.1(a)] is the numerical aperture of the beam. By substituting these values to the Eq. (2.7) and considering that the scaling factor is approximately calculated as $A \approx l/\rho$ one will get the formula for relative error of the measuring sys-

tem based on the spatial filtration of the dynamic speckles in the form:

$$\gamma = \frac{\lambda}{\pi \mathrm{NA}^{3/2} \sqrt{\rho L_S}}. \tag{2.8}$$

This equation can be used for estimation of the absolute error of measurements for both range sensors and the velocimeters. In the first case, the measurand is the distance ρ. Therefore, for range sensors the absolute error of measurements can be found as $\delta\rho = \rho\,\gamma$:

$$\delta\rho = \frac{\lambda}{\pi \mathrm{NA}^{3/2}} \sqrt{\frac{\rho}{L_S}}. \tag{2.9}$$

In the second case, the measurand is the surface velocity V. The surface displacement L_S is the product of the surface velocity V and the time of measurement T. Hence, for velocimeters the absolute error of measurement can be found as:

$$\delta V = V \cdot \gamma = \frac{\lambda}{\pi \mathrm{NA}^{3/2}} \sqrt{\frac{V}{\rho T}}. \tag{2.10}$$

2.3 TEMPORAL CHARACTERISTICS

In the previous subchapter the Eq. (2.8) was obtained under the assumption that in systems based on spatial filtration of dynamic speckles measurement inaccuracy originates from the uncertainty in the estimation of the speckle position, which is defined by the average speckle size. This accuracy limitation is imposed by the wave properties of the light and in this regard it is similar to the Rayleigh criterion for resolution of optical instruments [61]. As one can note, there are no temporal characteristics, such as speckle or surface velocities, in Eq. (2.8). In fact, the relative measurement accuracy is defined by just a few geometrical parameters of the optical setup. Nevertheless, it is also

clear that in order to achieve diffraction-limited accuracy operational speed of the receiving (photodetector and its amplifier) and data-processing parts of the system should be adequate to the temporal properties of the speckle pattern. Therefore, it is important to find the temporal parameters of the photodetector signal that correspond to the spatial characteristics of the speckle pattern defining the accuracy limits.

The spatial-temporal properties of the dynamic speckles can be described by several statistical parameters [54]. For a given speckle velocity, $V_S = A\,V$, it is possible to introduce a temporal parameter equivalent to the speckle translation length r_T: $\tau_{LT} = r_T/V_S = w/V$. This parameter is called as speckle lifetime. By using it the beam spot radius at the studied surface can be represented as $w = V\tau_{LT}$. Another temporal characteristic of the dynamic speckles called as coherence time of speckles, τ_C, was introduced by Yoshimura in [54] as

$$\frac{1}{\tau_C} = |V|\left(\frac{A^2}{r_S^2} + \frac{1}{w^2}\right)^{1/2}. \qquad (2.11)$$

Assuming that $r_T >> r_S$, as it usually is for the measuring systems with the spatial filtration of light, one can simplify the Eq. (2.11) to $\tau_C = r_S/V_S$. The coherence time of speckles defines the frequency bandwidth of the time-varying speckle-intensity fluctuations caused by the relative beam-surface displacement. Since the correlation function of these intensity fluctuations is a Gaussian function, the power spectrum of the fluctuations is also a Gaussian function. Frequency bandwidth of the later defined by the value of $1/e$ from the maximum is expressed as

$$f_S = (\pi\tau_C)^{-1} = V\,\mathrm{NA}/\lambda\,. \qquad (2.12)$$

Using the above temporal characteristics of the speckles and remembering that $L_S = V\,T$, one can rewrite Eq. (2.7) as

$$\gamma = \frac{\tau_C}{\sqrt{\tau_{LT}T}} = \frac{1}{\pi f_S\sqrt{\tau_{LT}T}}\,. \qquad (2.13)$$

Spatial filtration of the dynamic speckles by the spatial filter (e.g., optical grating, Ronchi rulings) results in periodical modulation of the filtered light intensity. Collection of this light by a convenient photodetector provides quasiperiodic electric signal whose central frequency is defined as

$$f_0 = \frac{V_S}{\Lambda} = \frac{AV}{\Lambda}, \tag{2.14}$$

where Λ is the period of the spatial filter. Typical oscilloscope trace of such a signal is shown in Fig. 2.2. This signal fragment was filtered by a band-pass filter in order to remove high frequency noise and influence of the low-frequency component of the signal.

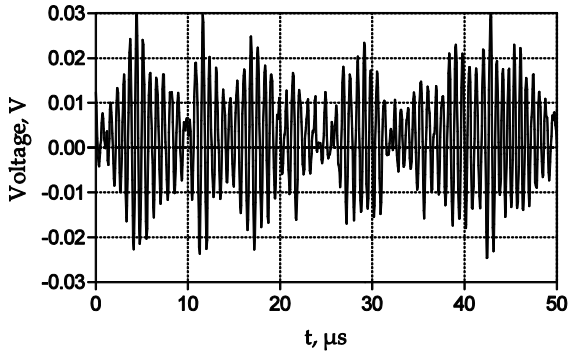

Figure 2.2 *Typical oscilloscope trace of the photodiode signal provided by spatially filtered dynamic speckles.*

According to Eq. (2.14), the central frequency of the photodetector signal f_0 depends on the scaling factor and the surface velocity. Consequently, similarly to the speckle translation distance L_T, it can be used in various applications for velocity or distance measurements. Analysis of the photodetector signal parameters defining the measurement accuracy can be done using the spectral description of that signal. Due to the stochastic nature of the dynamic speckles the photodiode signal is also stochastic. It represents itself as a random process whose spectral power density can be described by a Gaussian function [32]:

$$G(f) = \exp\left(-\frac{f^2}{f_D^2}\right) + \frac{1}{4}\exp\left(-\frac{\pi^2 r_S^2}{\Lambda^2}\right)\exp\left[-\frac{(f-f_0)^2}{f_D^2}\right], \quad (2.15)$$

or with substitution of r_S by $V_S/(\pi f_S)$:

$$G(f) = \exp\left(-\frac{f^2}{f_D^2}\right) + \frac{1}{4}\exp\left(-\frac{f_0^2}{f_S^2}\right)\exp\left[-\frac{(f-f_0)^2}{f_D^2}\right]. \quad (2.16)$$

Here $f_D=(\pi\tau_{CD})^{-1}$ is half of the signal bandwidth, defined by the correlation time τ_{CD}

$$\tau_{CD} = \frac{1}{V_S}\left(\frac{1}{r_T^2} + \frac{1}{D^2}\right)^{1/2}, \quad (2.17)$$

where D is the aperture size of the spatial filter from which the light is collected into the photodetector. Simple analysis of the Eq. (2.16) shows that increasing of the signal correlation time τ_{CD} leads to the narrower signal spectrum, and consequently to the higher accuracy of the estimation of the central frequency f_0. According to the Eq. (2.17), the correlation time approaches its maximum when $D \gg r_T$. If this condition is met, then the signal correlation time becomes equal to the speckle lifetime $\tau_{CD}=\tau_{LT}=r_T/V_S$.

Further analysis of the Eq. (2.16) shows that for a given speckle bandwidth f_S the power of the informative part of the signal spectrum decays rapidly with the increase of the central frequency f_0. On the one hand, this implies that the photodiode signal has a signal-to-noise ratio (SNR) sufficient for estimation of the signal frequency only if the central frequency does not exceed the speckle bandwidth, $f_0 \le f_S$. On the other hand, for a given signal bandwidth f_D accurate frequency estimation requires sufficiently high central signal frequency. Thus, in order to have a compromise between the SNR and the accuracy of the frequency estimations central signal frequency should be properly chosen. As one can see from the Eq. (2.16), power of the signal informative part decays e times at the condition $f_0=f_S$. Under the

assumption that in this case the SNR is high enough for proper data processing, using Eq. (2.13) one can calculate relative error of the frequency estimation as

$$\gamma = \frac{\sqrt{f_D}}{f_0\sqrt{\pi T}} \approx \frac{0.56}{f_0}\sqrt{\frac{f_D}{T}} \,. \tag{2.18}$$

Note that f_0 becomes equal to f_S when the grating period is π fold to the speckle size: $\Lambda = \pi r_S$.

2.4 ACCURACY OF SIGNAL FREQUENCY ESTIMATION

Just like Eq. (2.8), both Eqs. (2.13) and (2.18) can be used for estimation of diffraction-limited accuracy of the measuring systems based on the spatial filtration of dynamic speckles. However, the later equation was derived under the certain assumption concerning the SNR of the photodiode signal. Therefore, Eq. (2.18) cannot guarantee diffraction-limited accuracy estimations unless the processing of the photodetector signal provides the optimal evaluation of its frequency. Due to the signal randomness, a precise frequency measurement is not possible. The only option in this case is to use statistical evaluation of the frequency using one of the signal processing algorithms, such as zero-crossing technique [62,63], instantaneous frequency evaluation [64–66] or fast Fourier transform (FFT) [67,68]. But, independently of the signal processing technique, the signal itself possesses some statistical properties that impose certain restrictions on the accuracy of the estimation of its central frequency. These restrictions are very important since they are limiting the final accuracy of the measuring systems based on dynamic speckles. In addition these restrictions allow estimation of the signal processing efficiency and provide information necessary for optimization of the signal processing algorithm.

Restrictions imposed on the accuracy of the frequency estimation by the statistical properties of the signal can be found by

the theoretical analysis of the signal with known characteristics. Following the expression for the signal spectrum [see Eq. (2.16)] the higher band of the signal in time domain can be represented as a complex stochastic process $s(t)=a(t)\exp(2\pi i f_0 t)$, where the real part of $s(t)$ is the detected signal, f_0 is its central frequency, and $a(t)$ is a complex narrowband random process with the bandwidth of f_D. In time domain the stochastic nature of $a(t)$ is characterized by the correlation function $R(t)=2\sigma^2 r(t)$, where $r(t)$ is a covariance function and σ^2 is a variance of both real and imaginary parts of $a(t)$, which means that $2\sigma^2$ is the total power of the signal. According to the signal spectrum, the covariance function can be written as $r(t)=\exp(-t^2/\tau_{CD}^2)$, where τ_{CD} is the correlation time of the signal, which is equal to $(\pi f_D)^{-1}$.

The simplified evaluation of the signal frequency can be done under assumption that two signal samples separated by the interval of τ_{CD} are independent. It is important to note that the frequency information is obtained basically from the signal phase $f=(1/2\pi)\partial\varphi/\partial t$. If the assumption concerning the independence of the signal samples is valid, then the signal phase difference $\Delta\varphi$ between these samples can be supposed to be an arbitrary random value within the range from $-\pi$ to $+\pi$ with uniform probability distribution. Thus, the variance of random phase drift during the time of τ_{CD} is $\sigma_{\Delta\phi}^2=\pi^2/3$. The phase drift $\Delta\varphi$ corresponds to the signal frequency shift $\Delta f=\Delta\varphi/(2\pi\tau_{CD})$. Therefore, the quadratic mean of frequency fluctuations can be estimated as

$$\sigma_{\Delta f}=\frac{\sigma_{\Delta\phi}}{2\pi\tau_{CD}}=\frac{1}{\tau_{CD}\sqrt{12}}=\frac{\pi f_D}{\sqrt{12}}. \qquad (2.19)$$

Using Eq. (2.19) one can estimate fluctuations of the signal frequency during the time interval τ_{CD}. It is clear estimation of the signal frequency over much longer time interval $T=L_S/V$ has an averaging effect. In this case the fluctuations of the measured frequency value are attenuated. Assuming that the signal values sampled with an interval τ_{CD} are independent and number of re-

ceived samples during the measurement time T is $N = T/\tau_{CD}$, the frequency error taking the averaging into account is:

$$\sigma_{\Delta f,T} = \frac{\sigma_{\Delta f}}{\sqrt{N}} = \sqrt{\frac{\pi f_D}{12T}}\,. \tag{2.20}$$

This simplified evaluation of frequency variations provides only a rough estimation of system errors. However, this may be sufficient to calculate the approximate relative accuracy for sensors with spatial filtering:

$$\gamma_{SF} = \frac{1}{f_0}\sqrt{\frac{\pi f_D}{12T}} \approx \frac{0.51}{f_0}\sqrt{\frac{f_D}{T}}\,. \tag{2.21}$$

As one can see this value is close to the diffraction-limited relative error specified in Eq. (2.18). It means that the diffraction-limited accuracy can be preserved in systems with spatial filtering if proper signal processing is used for the mean frequency evaluation. It is necessary to note that in arrangements with the fixed spacing of the spatial filter, the condition $f_0 = f_S$ (and therefore the diffraction-limited accuracy) can be achieved only for a certain distance between the beam waist and the surface $\rho^* = l\lambda/(\Lambda\,\mathrm{NA})$. For other distances, the relative accuracy of sensors with spatial filtering can be calculated as

$$\gamma_{SF} = \gamma\,\frac{\rho}{\rho^*}, \tag{2.22}$$

where γ is the diffraction-limited relative accuracy defined by either of Eqs. (2.8) or (2.13). This discrepancy between the diffraction-limited accuracy and accuracy of the realistic measuring system is illustrated in Fig. 2.3. Both curves are calculated using following parameters of the measuring system: the laser wavelength $\lambda = 0.532$ μm, spatial filter spacing $\Lambda = 1000$ μm, relative beam-surface speed $V = 35$ m/s, total measurement time $T = 100$ μs and numerical aperture of the beam $\mathrm{NA} = 0.05$. Also, considering that distance from the beam waist to the observa-

tion plane, (l-ρ), is chosen to be equal to 75 mm, it easy to calculate that these curves intersect in the point $\rho^* = 0.8$ mm.

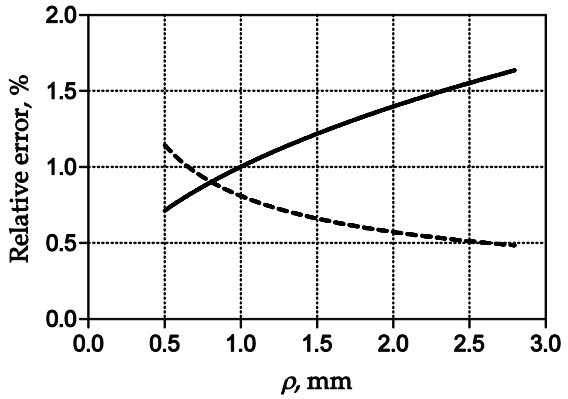

Figure 2.3 *Relative error of the mean frequency estimation as a function of the distance from the beam waist to the object surface. Solid curve is the accuracy calculated using Eq. (2.22); dashed curve is the diffraction-limited accuracy estimated by Eq. (2.8).*

Theoretical considerations presented in this chapter are supported by the experimental results. One can find these results and their detailed discussion in **Paper I**. It is necessary to make a special emphasis on one of important parts of the discussion. It was reported that accuracy of the measurements strongly depends on the quality of the illuminating wavefront. So, correlation time of the photodiode signal, $\tau_{CD} = w/V$, was 40% smaller than the theoretical expectations when the illuminating beam was formed by the corrected optics. This difference was threefold when the corrected optics was changed by the ordinary biconvex lenses. This discrepancy can be attributed to a deviation of the real wavefront of the illuminating beam from the perfect spherical shape which is mainly caused by aberrations of the used optical elements. Because of the spherical aberrations a smaller part of the surface participates in formation of coherent photodiode signal, which results in diminishing of the signal correlation time and increasing of the measurement error. Thus, in order to achieve maximal accuracy of the measurements in

addition to the proper data processing one should provide high quality wavefront of the illuminating beam.

3 Range sensor using micro-electro-mechanical deflector

Previous chapter was dedicated to estimation of theoretical limits of the measurement accuracy of diffraction velocimeters and range sensors. It was shown that accuracy of these measuring systems is defined solely by the geometrical parameters of the optical setup and the illumination beam. One should choose these parameters properly in order to achieve measurement accuracy close to the optimal one, limited only by the wave properties of the light itself. In comparison to the velocimeters and convenient range sensors, the scanning range sensors has additional component influencing the optimization process, namely, optical deflector. Besides defining such properties of the measuring system as scanning velocity, central frequency of the photodiode signal and length of the scan, the deflector imposes certain limitations on some properties of the illuminating beam. Surely, optimization of the optical setup should take the deflector into consideration, since qualities of this component influence performance of the whole system. Previous variations of the scanning range sensors were utilizing either acousto-optic deflector [33] or a fast-rotating mirror [34]. In addition to unique advantages and drawbacks, both of these deflector types are relatively expensive and do not provide sufficiently high fidelity required for routine measurements under harsh industrial environment. In this chapter novel design of a range sensor using scanning mirror based on the micro-electro-mechanical system (MEMS) technology for the laser beam deflection will be introduced. Since the MEMS deflector is much more compact and resistant to the mechanical influences than the rotating mirror,

and has a scanning angle much wider than the acousto-optic deflector, it can be considered as a good alternative to these deflectors. Moreover, due to the economies of scale, it is significantly cheaper than either of them. However, due to specific operational principle of this deflector, its applicability to the range sensing has to be verified. Original analysis of the MEMS scanner performance in the capacity of the range sensor deflector, and discussion of the data processing modifications related to the usage of this scanner will be given below.

3.1 RANGE SENSING USING THE MEMS SCANNER

Approximate layout of the dynamic-speckle range sensor using MEMS scanner as a deflector is presented in Fig. 3.1. Although the principles of the range sensing based on the spatial filtration of the dynamic speckles were described in the Chapter 2, it would be reasonable to remind some of them. In this method the distance evaluation is done through estimation of the central frequency of a quasiperiodical photodiode signal. According to Eq. (2.14), this frequency is defined by the ratio of the speckle pattern velocity in the observation plane, V_S, to the period of the spatial filter, Λ. Speckles velocity is connected with the velocity of the laser spot on the object, V, by the scaling factor, $A = l/\rho$, as

$$V_S = AV = V\frac{l}{\rho}, \tag{3.1}$$

where l and ρ are the distances from the object surface to the spatial filter and the beam waist, respectively. In the systems using the acousto-optic or mirror-drum deflectors the velocity of the scanning beam is usually constant. However, due to the operational principle of the MEMS scanning mirror, the beam velocity greatly varies during the scan. The velocity inconstancy arises from the fact that the mirror oscillations occur at the resonant frequency of the deflector mechanical structure, and the

mirror deflection angle θ_D varies in time in accordance with the sinusoidal law:

$$\theta_D(t) = \frac{\theta_{DF}}{2}\sin\Omega t\,, \tag{3.2}$$

where θ_{DF} is full (peak-to-peak) deflection angle, and Ω is MEMS resonant frequency.

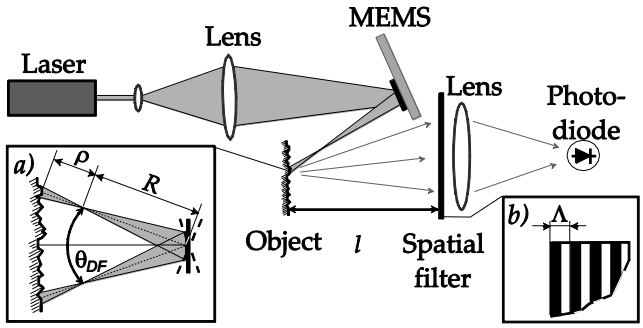

Figure 3.1 *Layout of the dynamic-speckle range sensor using MEMS scanner as a deflector. Inset (a) presents the geometry of the scanning which takes place in the plane perpendicular to the figure. Inset (b) presents a segment of the spatial filter. (Originally from* ***Paper II****)*

Since usually the distance from the mirror to the beam waist, R, is considerably bigger than that from the beam waist to the object surface, for simplicity reasons the velocity of the laser spot on the object surface can be supposed to be equal to the velocity of the beam waist, $V \approx V_{FS}$. It is easy to show that y position of the beam waist can be defined as $y(t) = R\sin\theta_D(t)$. The velocity of the beam waist can be found by taking the time derivative of this coordinate:

$$V_{FS}(t) = \frac{dy}{dt} = \frac{R\,\theta_{DF}\Omega}{2}\cos\Omega t\cos\left(\frac{\theta_{DF}}{2}\sin\Omega t\right). \tag{3.3}$$

In its turn, the distance ρ between the beam waist and the surface (in the direction of the beam propagation) can be presented as

$$\rho(t) = \frac{R + \rho_0}{\cos[\theta_D(t)]} - R, \tag{3.4}$$

where ρ_0 is the shortest distance from the beam waist to the surface. Substitution of Eqs. (3.3), (3.4) and (3.2) into Eq. (3.1) yields

$$V_{SP}(t) = \frac{R\,\theta_{DF}\Omega l \cos\Omega t \left[\cos\left(\frac{\theta_{DF}}{2}\sin\Omega t\right)\right]^2}{2\left\{\rho_0 + R\left[1 - \cos\left(\frac{\theta_{DF}}{2}\sin\Omega t\right)\right]\right\}}. \tag{3.5}$$

It is clear that following the speckle velocity the signal frequency f significantly varies during each half-period of beam deflections. As one can see, the frequency reaches its maximum when $\theta_D = 0$, at $t = j\pi/\Omega$, where j is integer:

$$f_{max} = \frac{R\theta_{DF}\Omega l}{2\,\rho_0}. \tag{3.6}$$

Variations of the signal frequency during a half of the period of MEMS oscillations calculated using Eqs. (2.14) and (3.5) for two values of parameter ρ_0 are shown in Fig. 3.2(a). As one can see, different distances between the beam waist and the surface provide the frequency traces clearly distinguishable from each other, which can be used for profile measurements. Nevertheless, the frequency changes significantly during a half of a scan. Consequently, for a proper signal processing and correct distance calculation one have to take this specific feature of the system with MEMS into consideration.

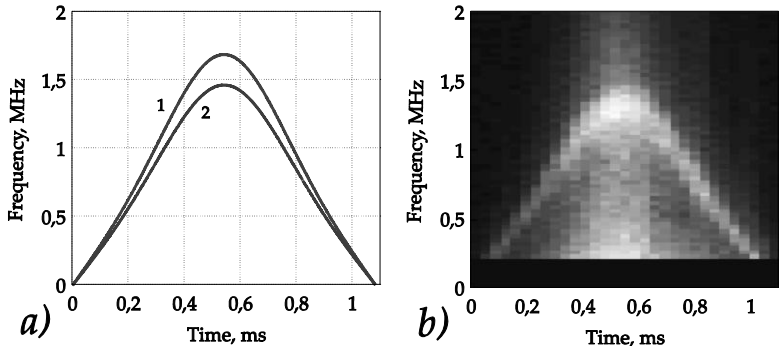

Figure 3.2 *Frequency variations during a half of the period of MEMS oscillations. (a) Theoretical calculations using Eq. (3.5) for ρ_0 = 3.42 mm (curve 1) and 4 mm (curve 2). (b) Averaged spectrogram of the 16 statistically independent photodiode signals along the scan. Each signal was recorded during a half of the period of MEMS oscillations at ρ_0 = 4 mm. Spectrogram was calculated from the signals using short-time Fourier transform with non-overlapping rectangular time windows of 32 μs. (Originally from* ***Paper II****)*

3.2 CHARACTERISTICS OF THE SIGNAL PROCESSING

Example of the oscilloscope trace of the photodiode signal provided by the setup employing the MEMS mirror (see Fig. 3.1), though too short to see the frequency variations, is presented in Fig. 3.3. Among the conventional methods used for frequency estimation of the stochastic signal, mentioned in section 2.4, the best results are usually provided by the spectral analysis employing FFT with further calculation of the central frequency. When the signal frequency is constant this method estimates the frequency value with the lowest random error. However, it provides poor results when the signal frequency changes along the scan. In this case, in order to achieve better results one can modify this method into time-frequency analysis using short-time Fourier transform (STFT) [69–71], which is typically used to obtain signals spectrograms. The average spectrogram illustrating the variations of the signal frequency along the scan is shown in Fig. 3.2(b). This spectrogram was obtained by processing of 16 statistically independent surface scans executed at the distance

ρ_0 = 4 mm by using STFT with non-overlapping rectangular time windows of 32 μs each. As can be seen, there is a good quantitative agreement between the spectrogram and the theoretical curve 2 in Fig. 3.2(a), calculated with the same parameter ρ_0. Therefore, the STFT can be considered as a suitable data processing method for such systems. But since the scanning range sensors typically have signals in the band of several MHz, implementation of the STFT will require quite sophisticated signal processing with high performance digital signal processors. Hence, so far it cannot be advised for practical applications in industrial environment due to strict hardware requirements. For similar reason, for the present the instantaneous frequency evaluation method cannot be considered as a suitable solution.

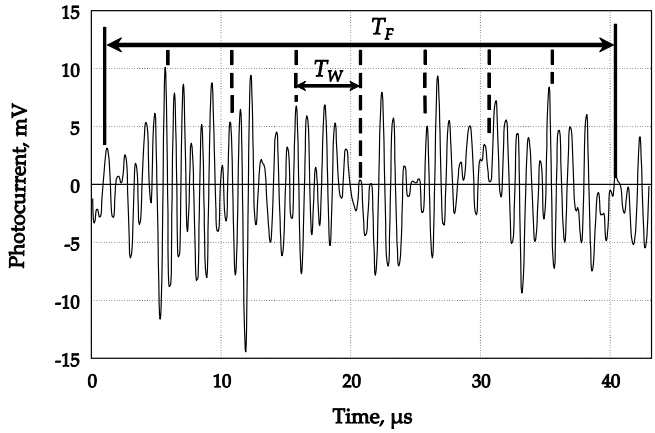

Figure 3.3 *Typical oscilloscope trace of the photodiode response with removed low frequency component obtained using the MEMS scanner, and example of the signal segmentation. (Originally from* ***Paper II****)*

In its turn, the zero-crossing (ZC) algorithm does not require any sophisticated calculations and according to the published data [60,72] provides the accuracy of frequency estimation (and, consequently, of distance measurements) sufficient for most of industrial needs. As suggested by its name, this method is based on counting the instances of the signal crossing the zero level (i.e., the sine signal normally crosses this level twice during each cycle). Normally, within a set measurement window T_F the signal with removed low-frequency component is divided into several segments of equal length T_W (as illustrated in Fig. 3.3),

and in each of these segments number of zero crossings is calculated. In order to diminish influence of the noise, only zero crossings of the signal with amplitude higher than 2-8 root mean squares (RMS) of the noise are counted. Moreover, as one can see from Fig. 3.3, due to the peculiarities of the signal there can be false or missing zero crossings. For that reason all the signal segments with the number of crossings outside of the specified interval are disregarded in the process of the frequency estimation. The average signal frequency is calculated as a ratio of the total number of valid zero crossings to the total length of valid segments. The results of application of this method to the signals obtained during a half period of MEMS oscillation at two distances from the beam waist to the object surface are shown in Fig. 3.4. The signals are processed using non-overlapping measurement widows (T_F = 32 μs) with a single segment in each and a different delay from the beginning of the scan.

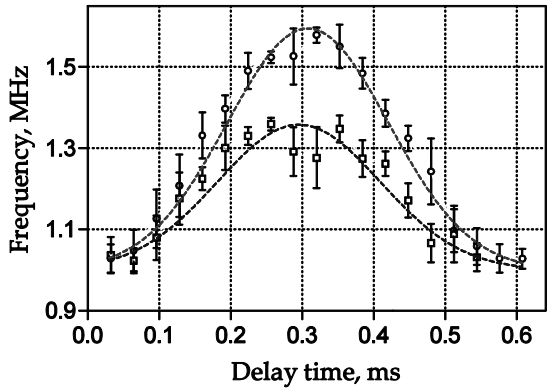

Figure 3.4 *Frequency estimated by zero-crossing method during a half of the period of MEMS oscillations for ρ_0 = 3.42 mm (circles) and ρ_0 = 4 mm (squares). Measurement window had only one segment of length T_F = 32 μs and variable delay from the start of the scan.*

As one can see, the frequency estimated by ZC technique is also in good agreement with theoretical calculations shown in Fig. 3.2(a). Due to the averaging, even in the center of the scan the estimated frequency is inevitably lower than the maximum frequency evaluated using Eq. (3.6). Nevertheless, it is im-

portant to note that unlike the photodetector noise or stochastic nature of dynamic speckles, the systematic variations of the frequency along the scan do not contribute to a random error of its estimation. Therefore, this systematic offset caused by the operational principle of the MEMS deflector can be neutralized after a proper calibration procedure. Consequently, usage of this type of deflectors does not compromise the accuracy of the scanning diffraction range sensors.

3.3 ACCURACY AND PROPERTIES OF ZC ALGORITHM

As was mentioned above, compensation of the frequency variations caused by the usage of the MEMS scanner requires calibration of the measuring system. The particular form of the calibration procedure is defined by the manner of the data acquisition. One of the ways is to use multiple measurement windows, as it was done to acquire data shown in Fig. 3.4. In this case it seems reasonable to retrieve shape of the frequency variance and find corresponding theoretical curve. Another approach is to use one big measurement window in the center of the scan, where according to Eq. (3.5) and Figs. 3.2 and 3.4 the frequency difference is highest for different distances ρ_0. In that case the single value of the averaged frequency should be set in correspondence with a certain distance. Although the former way appears to be a bit more accurate, the later one is much more computationally simpler. Therefore, it is more promising for practical applications.

In addition to the named frequency difference, the position of the measurement window is dictated by the quality of the signal. Due to certain features of the sensor scheme, quality of the photodiode signal decreases from the scan center to the borders. In other words, the photodiode signal obtained from the border of the scan has considerably more distortions leading to incorrect frequency evaluation by the ZC algorithm. As was mentioned in the previous section, poor signal quality can be compensated by dividing the measurement window into segments, calculating the frequency within each segment and dropping the

segments with inadequate frequency values. One can see the influence of the signal segmentation on the performance of ZC algorithm from Fig. 3.5, where are shown two series of measurements carried out for different distances (ρ_0 = 3.42 and 4.00 mm), for different lengths of measurement window (T_F = 256 and 512 μs) and with different lengths of the segments within the measurement windows ($T_W = 2^k$ μs, $k = 2, 3 .. 7$). As seen in Fig. 3.5, the mean signal frequency is practically independent from the parameters of the signal segmentation for both used lengths of the measurement window. Even for the smallest segment of 4 μs, which yields a bit higher frequency estimation, the difference from data obtained for other segmentations does not exceed the standard deviation of the measurements. Therefore, for the high quality signal, as provided by the central part of the scan, the signal segmentation does not influence the performance of the ZC algorithm.

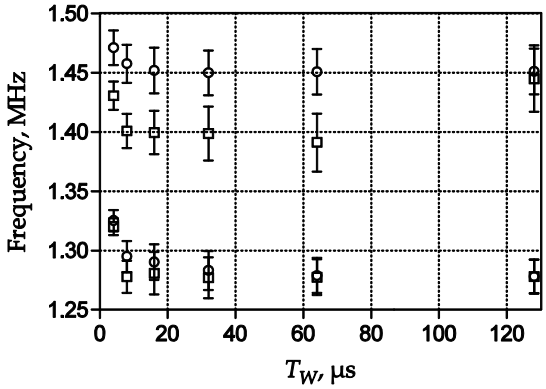

Figure 3.5 *Frequency estimated by ZC method for ρ_0 = 3.42 mm (upper points) and 4 mm (lower points) with measurement windows of T_F = 256 μs (circles) and 512 μs (squares). Measurement windows were centered at the middle of the scan.*

The data presented in Fig. 3.5 can be used for estimation of the accuracy of the distance measurements. As it was discussed in the Chapter 2 the relative error of the distance measurements is defined by that of the signal frequency estimation. For example, typically the measurand in profile measurements is the difference between two distances, $\Delta\rho = \rho_1 - \rho_2$. The relative measurement error of this parameter can be estimated as

$$\gamma = \frac{\sqrt{\sigma_1^2 + \sigma_2^2}}{|f_1 - f_2|}, \tag{3.7}$$

where $\sigma_{1,2}$ are experimentally determined standard deviations of frequency (shown as an error bars in Fig. 3.5) obtained from a single scan during a half-period of MEMS oscillations at ρ_1 = 3.42 mm and ρ_2 = 4.0 mm respectively, and $f_{1,2}$ are mean frequencies at these distances (points in Fig. 3.5). This relative error is shown in Fig. 3.6 as a function of the segments length. It is clear from this figure that the longer measurement window yields lower accuracy. The reason for this is the smaller frequency difference in the lateral parts of the scan coupled with the similar frequency fluctuations in the central and the lateral parts of the scan (see Fig. 3.4). Therefore, the shorter measurement window appears to be more suitable for profile measurements.

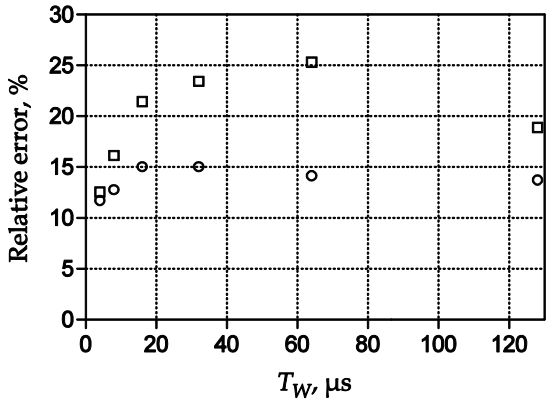

Figure 3.6 *Relative error of the distance measurements calculated using Eq. (3.7) for the measurement window of 256 μs (circles) and 512 μs (squares).*

The measurement accuracy can be improved by optimizing the parameters of the optical setup and averaging the results over a certain period of time. It was shown in Chapter 2 that the relative error is proportional to $NA^{-3/2}$. Therefore, increasing of NA of the scanning beam is one of the efficient ways to improve the accuracy. However, in case of the limited size of the optical deflector there is always a tradeoff between the working distance of the sensor and the NA of the scanning beam. Thus, at

the similar conditions the deflector with the larger surface and the higher scanning speed provides higher measurement accuracy.

Detailed description of the performed experiments and discussion of the experimental data are provided in **Paper II**.

4 Detection of small surface defects

The spatial filtration of dynamic speckles can be applied not only in the velocity measurements and range sensing. It was noted in Chapter 2 that imperfections of the illuminating beam wavefront results in the diminishing of the photodetector signal correlation time. In other words, deviation of the illuminating beam wavefront from the spherical shape results in the increase of the influence of the boiling type of the speckle dynamics. And the boiling speckles are prevailing in case of the surface illumination by a beam with completely distorted wavefront. However, when the radius of surface curvature is similar to that of the illuminating beam wavefront, even if the spherical shape of the wavefront is not distorted the surface illumination will yield the same effect. Small radius of the surface curvature usually signifies an abrupt change of the surface profile, which is typical for the surface defects (e.g., scratches, inclusions, cracks, holes, furrows, humps). Therefore, this can be used for detection of such defects.

Among the conventional optical methods developed for searching of the surface defects there are two that used most commonly. The first one is so called "machine vision" [73–75]. It is based on the analysis of the digital images of the inspected surface, and its biggest advantage is capability to inspect a big surface area at a time. But, since in order to be capable of on-line detection of fine defects the method requires digital camera with high resolution and frame rate, and large computational resources, the industrial detection systems based on this method are typically expensive and in many cases have low operational speed. The second method is based on the scanning of the surface by a laser beam [76–78]. The defects are detected through the analysis of the light scattered by the surface: intensity of the

light scattered from the defective surface region noticeably differs from that of the defect-free surface region. The operational speed and resolution provided by this method are typically high, but usually systems based on it are not suitable for universal usage. In particular, they require recalibration in case if any of the parameters influencing the intensity of scattered light (surface roughness, scattering coefficient of material, etc.) are changed. Furthermore, it is quite possible that the fluctuations of the laser's power or even presence of the dust can be a reason of false-positive response of the detection system.

Usage of spatially filtered dynamic speckles for surface defect detection can provide high operational speed and resolution combined with simplicity and reliability of measurements. This novel method utilizing spatial filtration of dynamic speckles for detection of small surface defects, the factors defining its resolution and a ways to achieve optimal performance will be discussed in the current chapter.

4.1 DESCRIPTION OF THE METHOD

As it was mentioned above, typically in the presence of a surface defect the type of the speckle pattern dynamics is changing from translating to boiling. Since the main difference between these types of speckle dynamics is in the mean velocity of the speckle pattern (see introduction of Chapter 2), one can reliably discern them by using the spatial filtration. As one should already know, only the translation type of the speckle dynamics provides periodically modulated photodiode signal after the spatial filtration. Thus, change of the type of speckle dynamics is manifested as a disappearance of that periodical modulation. Moreover, there is no periodical signal when the surface does not scatter the incident illumination, as it happens when the scattering surface is absent (in presence of a through hole), when the light is specularly reflected (e.g., in case of the scratch on the coated metal surface), or when the light is completely absorbed by the surface (e.g., in case of inclusion of a highly absorbing material).

All of these cases can be considered as defects. Therefore, the absence of the periodical modulation of the photodiode signal can be used as an indication of the surface defect presence.

However, presence of the surface defect is not the unique reason which can lead to irregular modulation of the output electrical signal of the photodiode. The temporal shape of the signal obtained by the spatial filtration of a single speckle is very close to pure sinusoidal. But, as it was mentioned in Chapter 2, individual speckles are statistically independent, that is each speckle has its own speed, shape and the lifetime. This results in the slightly different frequencies and phases of the signals provided by these speckles. Typically more than one speckle is collected into a photodiode. Thus, the photodiode response is a combination of a several sinusoids with a different phases and slightly different frequencies, and, as was discussed in Sect. 2.3, it is represented by a narrow-band random signal with the mean frequency f_0. Consequently, by increasing the number of speckles collected into the photodiode one will increase only the DC-level, while amplitude of the modulation term will be comparable with that for the case of collecting few speckles. This means that the small speckle ensembles (up to couple of tens of speckles [32]) can provide higher SNR than the larger ones [34]. Moreover, due to statistical difference of the collected speckles, even the photodiode signal obtained for a defect-free object surface has some drop outs in its regular modulation, and periodicity of these drops is characterized by the coherence time of dynamic speckles. Typically, the drops of the regular modulation in the signal obtained from the defect-free plain surface occur for no longer than 1 – 4 modulation periods. Therefore, absence of the regular modulation for longer than 10 periods can be associated with the presence of a surface defect in the scanned area.

One can see the difference between the photodiode responses recorded when the laser beam was scanning the defect-free surface area and the area containing the defect (non-through hole) from Fig. 4.1. Both signals were recorded under the exactly the same conditions using the setup typical for diffraction

velocimeters and range sensors. The signals were filtered by a band-pass filter in order to remove the non-informative low-frequency component and diminish influence of the high-frequency noise. In spite of the fact that the conditions were the same, there is a big difference between these traces. The signal obtained from the defect-free surface [Fig. 4.1(a)] has quasi periodical character with random phase variations, which is typical for the spatially filtered dynamic speckles (compare with Figs. 2.2 and 3.3). It is clearly seen from this figure that the wave trains with the average length equal to the coherence length of speckles, τ_C, have between them several short phase failures caused by the stochastic nature of speckles. In contrast, the signal obtained by scanning of the surface containing the defect [Fig 4.1(b)] has no regular modulation for a much longer period of time. The length of this time period is in the excellent correspondence with the defect size and the velocity of the laser beam. The scanning was organized so that the laser spot diameter was equal to the diameter of non-through hole used as a sample of the surface defect, and the center of the spot was crossing the defect center. Therefore, the long absence of the periodically modulated signal indeed can be used as an indication of the surface defect presence.

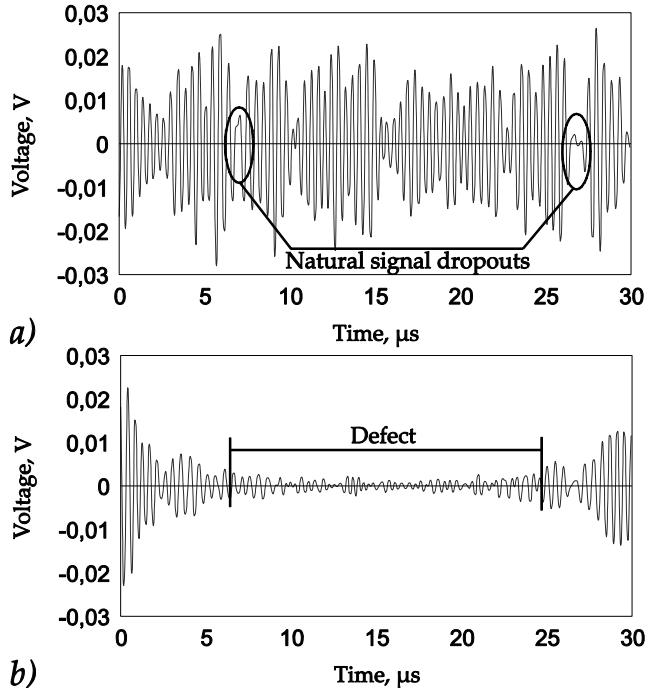

Figure 4.1 *Oscilloscope traces obtained by scanning (a) defect-free surface and (b) surface area containing the defect (non-through hole with diameter equal to that of the laser spot on the surface).*

4.2 RESOLUTION OF THE TECHNIQUE

In the previous section it was shown how the spatial filtration of the dynamic speckles can be used for detection of the surface defects. Now it is necessary to discuss the parameters defining resolution of that technique. Since it was proposed above to use absence of 10 or more periods of the photodiode signal periodical modulation as a criterion of the surface defect detection, the first of these parameters is the laser beam displacement which is needed to provide one period of the photodiodes signal modulation. Indeed, in case if the defect size in the direction of the scanning is smaller than ten such displacement distances, then under the current conditions that defect is non-detectable by means of the discussed technique. That parameter can be easily derived using Eq. (2.14) as:

$$\Delta x = \frac{V}{f_0} = \frac{\Lambda}{A}. \tag{4.1}$$

As it was discussed in Chapter 2, since relation $l >> \rho$ is valid for the majority of measuring systems based on the spatial filtration of dynamic speckles, the scaling factor can be approximated as $A \approx l/\rho$. Considering that the average speckle size can be calculated as $r_S = l\lambda/(\pi\rho\mathrm{NA})$, Eq. (4.1) can be rewritten as

$$\Delta x = \frac{M \cdot \lambda}{\pi \cdot NA}, \tag{4.2}$$

where M is the ratio Λ/r_S, which will be called here as a scaling coefficient. As it was shown in Section 2.3, the SNR of the photodiode signal has acceptable values when the condition $M \geq \pi$ is fulfilled. Moreover, the scaling coefficient should not be very large, since according to Eq. (4.2) the resolution of the discussed technique is inversely proportional to it. Therefore, it seems reasonable to keep its value in the range from π to 2π.

The second parameter defining the resolution is the beam radius at the object surface, $w = \rho\mathrm{NA}$. As it was noted in section 4.1, presence or absence of the regularly modulated photodiode signal is defined by the type of speckle pattern motion: translation or boiling, respectively. And the speckle motion inevitably becomes boiling when the average curvature of the scanned surface is comparable with the wavefront curvature of the illuminating beam. The speckles are formed by the light scattered from the whole illuminated area. In case when this area is sufficiently larger than the defect, some part of the defect-free area is permanently scanned providing translational speckles in quantities necessary for formation of the regularly modulated photodiode signal. In other words, smallest detectable defect size is in the direct relation with the size of the illumination spot.

Thus, the resolution of discussed technique depends on both the surface shift necessary for formation of one modulation period and the radius of the laser spot on the studied surface. It is easy to see that numerical aperture of the illuminating beam,

NA, and distance from the beam waist to the surface, ρ, have influence on both of these parameters. And while reduction of the later results in decrease of Δx as well as w, the former property influence these parameters differently. So increasing of only the beam numerical aperture will multiply number of the modulation periods produced by scanning of the unit of surface (thus increasing the resolution) and enlarge the size of the laser spot on the surface (which decrease the resolution). Therefore, depending on the requirements imposed on the measuring system this parameter of the optical setup should be always optimized. Moreover, one should remember that in order to keep SNR at the high enough level, any changes of the illumination spot size should be done together with the proper adjustment of the period and/or position of the spatial filter.

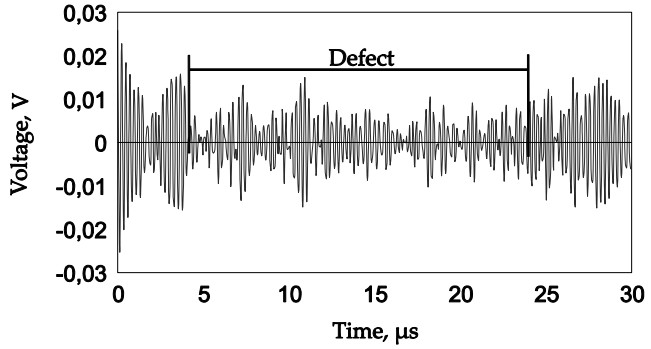

Figure 4.2 *Oscilloscope trace obtained by scanning surface area containing the defect (non-through hole with diameter twice smaller than that of the laser spot on the surface).*

The photodiode response shown in Fig. 4.2 is received from the same surface area and with the same value of ρ as the response from Fig. 4.1(b). But in this case the numerical aperture of the beam was doubled in order to show how parameters w and Δx influence the technique resolution. As one can see, the modulation frequency of the signal presented in Fig. 4.2 is higher than that of the signals shown in Fig. 4.1. It shows that the value of Δx has decreased and scanning of the same surface area produces more periods of the signal modulation. It should be noted that both the spacing and position of the spatial filter were adjusted in order to compensate for growth of the illumi-

nation spot and keep the SNR at the high enough level. That has leaded to slight increase of the scaling coefficient M, and, consequently, the difference between the frequencies of the signals shown in Figs. 4.1 and 4.2 is less than twofold. However, since increasing of the beam numerical aperture has made the illuminating spot twice bigger than the defect, the photodiode signal remains periodically modulated even when the laser spot crosses the defect center. Therefore, in process of the measuring system design one should always try to optimize values of both Δx and w.

Along with detailed description of the performed experiments one can find description of the prototype of the defect detection system based on proposed technique and discussion of its performance in **Paper III**.

5 Estimation of light penetration depth in turbid media

The speckle effect can be observed from virtually any material. Therefore, methods and techniques presented in the previous chapters can be used in a very wide range of industrial applications. For example, it was shown [**Paper IV**] that in case of the turbid media with a rough fast-moving surface range sensing based on the spatial filtration of the dynamic speckles has certain advantages and can potentially compete even with the optical triangulation methods [79]. However, in every particular case of using dynamic speckles formed by the turbid medium it is necessary to take into account influence of the speckles formed by the light scattered from within the material. In order to do that it is essential to know how deep the light penetrates into the material. But in contrast to a medium with negligible internal scattering, where the light penetration depth (LPD) can be found using Beer-Lambert law, there is no simple solution for LPD estimation in turbid media.

The most widely used method for estimation of LPD in materials with internal scattering is the Monte Carlo simulation [80,81]. This computational method can predict behavior of the light in the medium with very high precision, but it requires high computational resources and knowledge of scattering, absorption and reflection coefficients of the studied material. Various analytical methods were developed in order to diminish the computational burden [82–84]. But, their computational simplicity is usually achieved at the expense of prediction precision, and in some cases they are accurate only under certain conditions. Just like the Monte-Carlo method, analytical

methods need knowledge of the medium optical properties. In many cases assessing of these parameters can be troublesome. Considering this fact, for approximate estimation of the LPD one can prefer some simple experimental technique.

One of the few experimental methods for estimation of LPD in turbid media was proposed by Xie et al. [85]. It is based on direct measurements of the fluence rate inside the material by means of the optical-fiber probe inserted into the needle. The needle is introduced into the material from the side opposite to the one illuminated by a laser. Insertion depth can be adjusted using the micrometric translation stage, thus allowing recovery of the fluence rate depth profile. The material LPD is estimated by fitting the exponential function to that profile. This method is very simple and straightforward, but due to its operation principle it is destructive and inapplicable to the hard materials. Another experimental method described in [86] is based on the analysis of the light backscattered from the medium. Two normally oriented multimode optical fibers situated right against the sample surface are used as the point light source and detecting probe, respectively. On the basis of the distance from the source to the detector one can assess the maximal depth from which the detected light has come by using simple analytical formula. Thus, the LPD can be estimated by finding such a source-detector distance that the power of detected light is e times decayed in respect to that of the light introduced into the material. In addition to simplicity, this method is non-destructive. However, it is applicable only to the homogenous scattering media with low absorption, and can provide only rough LPD estimation.

Thus, there is a need for simple non-contact and non-destructive method for estimation of the turbid media LPD. In this chapter novel experimental method for LPD estimation will be demonstrated. Method is based on the analysis of the spatial structure variations of the speckle patterns formed by coherent illumination of the turbid media. An original theoretical model treating the light scattering in the turbid media as a reconstruction of the thick hologram will also be introduced here.

5.1 SPECKLE EFFECT FOR TURBID MEDIA LPD ESTIMATION

As known, a speckle pattern is an intensity distribution produced by the mutual interference of a large number of waves scattered by the object [87]. In case of the turbid media, which in general can be represented as a random set of the scattering centers, these waves are scattered from the surface as well as from the bulk of the material. When a certain condition is met, by tilting the illuminating beam in respect to the material surface one can separate influence of the surface and inner scatterers on the formation of the resulting speckle pattern. It can be done when the laser spot position on the surface is fixed during the beam tilting. For that the axis around which the beam (or the object) is rotated should be placed on the object surface crossing the illuminating spot centre. Tilt of the illumination beam in respect to the object surface will result in the change of phase differences between waves reflected from a large number of scatterers situated within the material, while the phases of the waves scattered from the surface will remain almost unchanged. Therefore, during the beam tilting some part of the speckle pattern will remain almost changeless, while the other part of the pattern will change considerably. And the magnitude of these changes is directly related to the material LPD. Thus, by tracking changes of the spatial structure of the speckle pattern one can estimate LPD of the medium.

Generally speaking, formation of the speckle pattern by the interference of a large number of scattered waves can be approximated as reconstruction of the hologram recorded by the incident beam as a reference wave with that speckle pattern as an object. In this case the difference between the surface and volume scattering can be attributed to the different kinds of the holograms: thin and thick [88]. The sample surface can be considered as a thin hologram which does not have strong angular selectivity. Thus, independently of the illumination angle changes some part of the speckle pattern will maintain its spatial structure. In their turn, the speckles formed by the light scattered inside the material can be considered as the original object

wavefront obtained by reconstruction of a volume hologram. Just like the thickness of the volume hologram defines its angular selectivity, the range of incidence angles of the illuminating beam within which the varying part of the speckle pattern still maintains its fine structure depends on the mean free photon path in turbid media.

In any case, the observed speckle pattern is formed by the light backscattered/diffracted from both the surface and inside of the object. It would be correct to say that each layer of the material participates in the formation of the pattern by returning part of the incident light back to the observation plane. In the isotropic turbid media intensity of the incident light wave is exponentially attenuated due to absorption and scattering processes. At the depth of z it can be computed as:

$$I = I_0 e^{-\frac{z}{Z}} = E_0^2 e^{-\frac{z}{Z}}, \tag{5.1}$$

where I_0 and E_0 are the intensity and the amplitude of the incident light at the surface, respectively, and Z is the depth at which the light intensity is e times smaller than at the surface. In other words, the parameter Z is an effective LPD. Usually single material layer reflects only a small fraction of the incident illumination. Naturally, on its way to the object surface light is once again attenuated. Thus, the small increment of the backscattered light amplitude provided by the layer situated on the depth z can be estimated as

$$\delta E_R \propto E_0 e^{-\frac{z}{Z}}. \tag{5.2}$$

Representation of the turbid media as a random thick hologram with low diffractive efficiency will be adequate to the above reasoning on condition that the incident wave has low attenuation or even does not decay, but the hologram itself is not uniform in z-direction and modulated by the factor $e^{-z/Z}$. In this case the increment of the amplitude of the diffracted light wave from the depth z is also defined by the Eq. (5.2). The angular se-

lectivity of such a hologram can be illustrated by the well known method of Ewald spheres [89]. In Fig. 5.1 are shown all light waves and the hologram in a spatial-frequency domain. Two circles with the radiuses of $2\pi/\lambda$ and $2\pi n/\lambda$, where n is the material refractive index, are representing Ewald spheres for all possible light waves in the air and medium, respectively. Two vectors pointing up-left are representing incident and refracted waves prior to the object rotation, and the horizontal vector pointing right is a wave diffracted from the hologram. The hologram vector is denoted as $\vec{K}$. Angles θ and θ_n are incidence angles in the air and in the medium, respectively. In their turn, angles $\delta\theta$ and $\delta\theta_n$ show the change of the incidence angles due to the beam tilting. As one can see from the Fig. 5.1 incidence and refraction angles are in exact correspondence with the Snell's law.

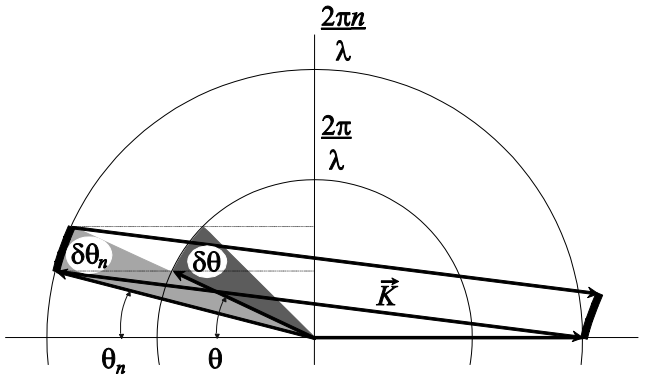

Figure 5.1 *Schematic representation of the diffraction from the thick hologram in spatial-frequency domain. Circles with the radiuses of $2\pi/\lambda$ and $2\pi n/\lambda$ are representing Ewald spheres for all possible light waves in the air and medium, respectively. Angles θ and $\delta\theta$ are incidence angle and its change due to rotation in the air, while θ_n and $\delta\theta_n$ – in the medium. Two vectors pointing up-left are representing incident and refracted waves. The horizontal vector pointing right is a diffracted wave. Vector denoted as $\vec{K}$ is a hologram vector. (Originally from* ***Paper V****)*

In this coordinate system, fulfillment of the Bragg's law for thick holograms requires coincidence of end points of the incident and diffracted wave vectors with the end points of the grating vector. In the ideal case the grating vector has a fixed length, and light diffraction from the hologram is possible only at a cer-

tain angle of incidence. However, due to the finite thickness of the hologram there always is small uncertainty in the grating vector length. As a result, the light can be diffracted at some set of incidence angles with the efficiency defined by the proximity of the incidence angle to the Bragg angle. Unlike the light waves, the hologram is fixed in respect to the object and its vector cannot be rotated. It is easy to see that change of the incidence angle by $\delta\theta$ causes rotation of the wave vector corresponding to the refracted beam by $\delta\theta_n$. Owing to the rotation the end-point of this vector follows the arc shown in Fig. 5.1 by a thick line. Since the end-points of the incident and the grating vectors should coincide and the hologram vector cannot be rotated, when the incidence angle is changed the right end-point of the vector $\vec{K}$ also follows the arc, going out of the sphere of possible positions for the reconstructed wave. It leads to the Bragg condition mismatch. As a measure of this mismatch can be used horizontal displacement ζ of the grating vector end-point in respect to the end-point of the diffracted wave vector. Due to the mentioned properties of the hologram vector, the horizontal coordinates of left and right end-points of the vector $\vec{K}$ are changing in the same way. Thus, for simplicity here will be considered coordinate of the left end-point, which is defined as:

$$-\frac{2\pi n}{\lambda}\cos\theta_n = -\frac{2\pi n}{\lambda}\sqrt{1-\sin^2\theta_n} = -\frac{2\pi n}{\lambda}\sqrt{1-\frac{\sin^2\theta}{n^2}}. \quad (5.3)$$

Shift of the end-point caused by the change of the illumination angle on $\delta\theta$ can be defined through differentiation of the Eq. (5.3) with respect to the angle:

$$\zeta = \frac{2\pi\,\delta\theta\sin 2\theta}{\lambda\sqrt{4n^2-2+2\cos 2\theta}}. \quad (5.4)$$

The space-frequency domain is nothing else but the Fourier domain. Therefore, considering the introduced mismatch pa-

rameter, the relative amplitude of the reconstructed hologram can be evaluated as:

$$E(\zeta) = \int_0^\infty e^{-\frac{z}{Z}} e^{-i\zeta z} dz = \frac{Z}{1 + i\zeta Z}. \tag{5.5}$$

And the intensity of the reconstructed wave is proportional to the square modulus of this equation:

$$I_R \propto \frac{Z^2}{1 + \zeta^2 Z^2}. \tag{5.6}$$

As was mentioned above, formation of the speckle pattern can be considered as a hologram reconstruction. Therefore, change of the speckle pattern spatial structure caused by beam tilting (or the object rotation) can be regarded as weakening of the initial hologram due to the mismatch from the Bragg condition by the parameter ζ in the spatial frequency domain. In this case the maximum of the correlation function calculated for two speckle pattern snapshots taken before and after the object rotation should also obey Eq. (5.6). And equation describing the dependence of the correlation function amplitude on the illumination angle can be obtained by substituting Eq. (5.4) into Eq. (5.6).

5.2 DISCUSSION OF THE METHOD

Equation derived in the previous section describes relations between the correlation function maximum and the illumination angle only for the speckles formed by the light backscattered from inside the material. As it was mentioned above, any optically rough surface can be considered as a thin hologram with low angular selectivity. The spatial structure of the speckle pattern formed by the surface scattering is almost independent of the changes of the incidence angle. However, change of the illumination angle causes shift of such a speckle pattern in respect to the fixed observer. In terms of the correlation function maxi-

mum, shift of the constant speckle pattern in respect to the fixed camera taking snapshots of that pattern results in the linear decline of the correlation peak amplitude. The behavior of light scattered from the surface is identical for materials with surface-only scattering (e.g., metals) and for materials with internal scattering (e.g., semitransparent plastics). Therefore, while in the former case the correlation peak will decline linearly along with the change of the angle, in the later case the correlation function amplitude will have bell-shaped decay in the area of small angle changes and linear decay in the area of large angle changes. Dependencies of the correlation function amplitude on the illumination angle for materials with different properties are presented in Fig. 5.2.

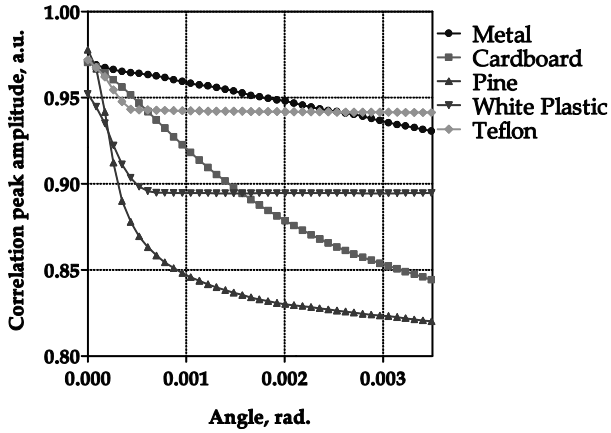

Figure 5.2 *Correlation peak amplitude versus change of illumination angle measured for different materials. (Originally from* ***Paper V****)*

As one can see, while graphs of semitransparent materials with both low (white plastic and Teflon) and high (cardboard and pine wood) absorption have a certain similarity, in accordance with the theory they have a noticeable difference with the graph of the material without internal scattering (metal). The graphs representing turbid media are clearly nonlinear and, at least in the region of small angle changes, decline much faster than the graph representing the metal. Moreover, as expected, the rate of the graph decline is directly proportional to the material LPD. As an example can be compared graphs of the card-

board and the Teflon. Due to the high absorption, optical penetration depth in the cardboard is very small. Therefore, the speckle pattern in the observation plane is formed by the light scattered from the material surface and layers situated in its immediate vicinity. Consequently, the dependence of the spatial structure of this pattern on the illumination angle is manifested weakly, which is displayed by the graph. In contrast to the cardboard, optical absorption in the Teflon is considerably lower, while the LPD is much larger. Therefore, variation of the illumination angle causes significant changes in the spatial structure of the speckle pattern formed by the Teflon. This leads to a rapid decrease of the amplitude of the correlation function maximum within a relatively small range of angles. In principle, outside of this range influence of the inner scattering on the correlation function should be negligible, and the graph shape should become linear. However, graph of both samples with low absorption and large LPD are almost constant after some angle. Nonetheless, although absence of the linear decline cannot be explained in the context of combination of inner and surface scattering, this fact does not compromise the method, since only a region of small angle changes is relevant for LPD estimation.

So the material LPD can be estimated judging by the width of the corresponding graph. It can be done numerically by fitting a proper function into the experimental data. Influence of the inner scattering on the correlation function has been discussed in the previous section. In its turn, influence of surface scattering can be described by the linear equation in a slope–intercept form. Thus, the dependence of the correlation function maximum on the illumination angle is described by the following formula:

$$C = \frac{C_0}{1 + \zeta^2 Z^2} + c \cdot \delta\theta + d\,, \tag{5.7}$$

where C_0 is the autocorrelation function amplitude, Z is the effective LPD, ζ is a term accounting the alteration of speckles related to the inner scattering caused by the illumination angle

change, $\delta\theta$ is the illumination angle change, c is the slope of the linear decline corresponding to the surface scattering, and d is the constant. Fitting of this function to the experimental data becomes much simpler after following variable transformations:

$$\zeta = \zeta_1 \delta\theta; \quad b^2 = \frac{C_0}{\zeta_1^2 Z^2}; \quad a^2 = \frac{1}{\zeta_1^2 Z^2}. \tag{5.8}$$

Substitution of Eqs. (5.8) into Eq. (5.7) gives following fit model:

$$C = \frac{b^2}{a^2 + \delta\theta^2} + c \cdot \delta\theta + d, \tag{5.9}$$

where a, b, c and d are the model parameters, and $\delta\theta$ is the independent variable.

By finding these parameters one can easily exclude influence of the surface scattering and analyze separately the behavior of internally scattered light as a function of the illumination angle. Dependences of the correlation function amplitude from the illumination angle for speckle patterns formed by the light scattered inside different materials are shown in Fig. 5.3. As one can see from this figure, after exclusion of the surface scattering influence the graph representing the metal became a straight line coinciding with the abscissa axis, which confirms that according to the discussed method there is no LPD in the metal. In their turn, graphs corresponding to the semitransparent materials show that the smallest LPD is in the cardboard, while the largest one is in the Teflon. The decrease of the amplitude of the graph with the growth of LPD can be easily explained, since the magnitude of the speckle pattern variation is directly proportional to the penetration depth, and smaller angle change is required for complete decorrelation. In other words, there is possibility that at very high values of the LPD even very fine change of the illumination angle can lead to complete change of the spatial structure of the speckle pattern formed by the internally scattered light. This can be avoided by increasing angular resolution of the measuring system. Thus, it is advisable to always opti-

mize the system resolution with respect to the optical properties of the studied material.

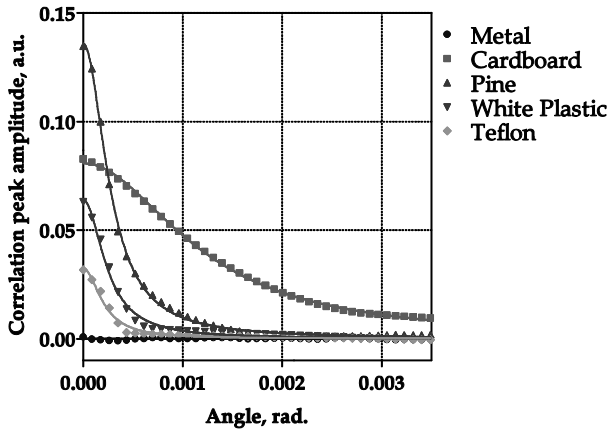

Figure 5.3 *Correlation peak amplitude versus change of illumination angle only for the light scattered inside the material. Dots are representing the experimental data, while solid lines – least squares fitting. (Originally from* ***Paper V****)*

As one can see, it is possible to qualitatively compare LPD of different materials judging by the width of the graphs shown in Fig. 5.3. But this width can be also used for quantitative estimation of the material LPD. In the model described by Eq. (5.9) width of the bell-shaped function is defined by the parameter *a*. If the refractive index of the studied material is known one can calculate penetration depth using Eq. (5.8) as:

$$Z = \frac{1}{\zeta_1 a} = \frac{1}{a}\frac{\lambda\sqrt{4n^2 - 2 + 2\cos 2\theta}}{2\pi \sin 2\theta}. \qquad (5.10)$$

It is clear from Eq. (5.10) that coefficient $1/a$ have the same order of magnitude as the ratio of effective penetration depth to the wavelength of the illuminating beam. In other words, it approximately shows effective LPD expressed in wavelengths of the incident light. The reciprocal values of the parameter *a* for semi-transparent materials are presented in Table 1.

***Table 1**. Reciprocal value of the parameter **a** for different materials*

Material	1/*a*
Cardboard	834.44
Pine wood	3596.58
White plastic	4056.03
Teflon	4768.94

Unfortunately, optical properties of turbid media are not widely reported. Among the listed materials, there is trustworthy information only about Teflon PTFE: its refractive index was reported to be approximately 1.35 at the wavelength of 633 nm. Consequently, the value of the Teflon LPD according to the discussed method is equal to 1.39 mm. However, this value cannot be compared with the published data because the search for LPD value of the Teflon in the visible range was unsuccessful. Results published in **Paper VI** can be used as a reference. In this work the effective LPD of the Teflon reported as 0.78 mm was estimated using method mentioned in the introduction to this chapter [86]. This method provides only approximate results. Therefore, since the difference between the results is less than twofold, one can consider the later result as a support of the feasibility of discussed method.

Certainly, there is a need for further studies. Here only a rough model describing the light scattering in the turbid media as a reconstruction of the thick hologram was presented. At the moment this model cannot explain behavior of the graphs corresponding to the highly scattering materials with low optical absorption in the region of large angle changes. Moreover, it is only partly applicable to the anisotropic materials and in this regard it is far from being complete. Also necessity of refractive index value for quantitative LPD estimation could be considered as a method limitation. However, it was shown that qualitative estimation of the LPD does not require knowledge of any optical properties of the material. Moreover, the refractive index of the turbid media can be measured by variety of methods, see for example [85,90]. The discussed method is simple, versatile, non-

contact and non-destructive. Therefore, it appears to be very promising.

Detailed description of the performed experiments and data processing algorithm, and discussion of the experimental data are provided in **Paper V**.

6 Summary

The goal of this work is development of new simple and reliable optical measuring systems based on dynamic speckles and improvement of existing systems.

We presented novel method for estimation of light penetration depth (LPD) in turbid media. The method utilizes strong dependence of the speckle pattern spatial structure on the light backscattered from within the material. We proposed here simple theoretical model based on the theory of Bragg diffraction from volume holograms which describes structural changes of the speckle pattern caused by the variation of the illumination conditions with reasonable precision. It was demonstrated here that the proposed model allows quantitative estimation of the LPD if only one optical parameter of the turbid medium (namely, the refractive index) is known, while there is no need for any material properties for qualitative LPD estimation. The method is relatively simple, fast, non-contact and non-destructive. Results provided by the proposed method (see **Paper VI**) are in good agreement with the results obtained by using alternative experimental method.

We presented in the Thesis another original experimental method allowing detection of small surface defects of nontransparent materials. The detection is done through analysis of the light intensity modulation caused by the spatial filtering of dynamic speckles. We demonstrated that the periodical modulation of the spatially filtered scattered light (which is typical when any optically rough surface is fast scanned by the laser beam) disappears when the radius of the surface curvature is comparable with the wavefront radius of the illuminating beam, which is typical for the surface defects. We proposed to use this observation as an indicator of the defects. It was shown that the resolution of the proposed method is defined solely by the geometrical parameters of the optical setup. Due to its operational

principle this method is immune to the optical noise with the frequencies lower than that of the high-frequency periodical intensity modulation. Practicability of proposed method was demonstrated by experimental results and by the prototype of the defect detection system reported in **Paper III**.

Also, we presented theoretical analysis of the fundamental accuracy limits of the measuring systems based on spatial filtration of dynamic speckles (such as velocimeters and range sensors) induced by the stochastic nature of speckles, which has shown that the maximal measurement accuracy of these systems is defined only by the geometrical parameters of the optical setup. We demonstrate that in the realistic measurement systems the theoretical accuracy limit can be reached with the proper data processing algorithms. Validity of the theoretical analysis is supported by the experimental results (see **Paper I)**. The developed theory can prove as a useful tool for estimation of the achievable accuracy of a particular measuring system based on spatial filtration of dynamic speckles, identification of the factors restraining the system performance, and optimization of the system design so that the system components are matched with each other to provide the highest possible performance.

Besides, we proposed to use a micro-electro-mechanical system (MEMS) mirror as a deflector in the dynamic speckles range sensor (see **Paper II**). We demonstrated that systematic variation of the scanning speed originating from the operational principle of the MEMS mirror does not compromise the measurements accuracy. It was shown that the analytical expression developed for depiction of system response to the varying scanning speed is in the good agreement with the experimental results. For the signal processing we proposed to use fast, simple and reliable ZC technique. Also, we briefly discussed the parameters of the optical setup and the signal processing which are crucial for optimization of the system performance.

This thesis showed that there is still potential for improvement of existing and development of completely new laser speckle applications. From the technical point of view, two original measurement systems for LPD estimation and surface de-

fect detection, as well as new modification of the dynamic speckles range sensor, were designed, developed and tested. All of these systems have proved to be simple, reliable and cost-efficient. From the theoretical point of view, fundamental accuracy limits of the systems utilizing spatial filtration of laser speckles and ways to optimize performance of these systems were analyzed.

References

[1] K. Thyagarajan and A. Ghatak, *Lasers: Fundamentals and Applications* (Springer, 2010).

[2] W. Liu and C. Zhou, "Femtosecond laser speckles," Applied Optics **44**, 6506–6510 (2005).

[3] J. W. Goodman, "Some fundamental properties of speckle," Journal of the Optical Society of America **66**, 1145–1150 (1976).

[4] E. N. Leith and J. Upatnieks, "Wavefront reconstruction with diffused illumination and three-dimensional objects," Journal of the Optical Society of America **54**, 1295–1301 (1964).

[5] W. Martienssen and S. Spiller, "Holographic reconstruction without granulation," Physics Letters A **24**, 126–128 (1967).

[6] J. C. Dainty and W. T. Welford, "Reduction of speckle in image plane hologram reconstruction by moving pupils," Optics Communications **3**, 289–294 (1971).

[7] F. T. S. Yu and E. Y. Wang, "Speckle reduction in holography by means of random spatial sampling," Applied Optics **12**, 1656–1659 (1973).

[8] P. Hariharan and Z. S. Hegedus, "Reduction of speckle in coherent imaging by spatial frequency sampling. II. Random spatial frequency sampling," Optica Acta **21**, 683–695 (1974).

[9] P. Hariharan and Z. S. Hegedus, "Reduction of speckle in coherent imaging by spatial frequency sampling," Optica Acta **21**, 345–356 (1974).

[10] M. A. M. Gama, "Speckle reduction by unidirectional averaging," Optica Acta **22**, 725–730 (1975).

[11] N. George and A. Jain, "Speckle reduction using multiple tones of illumination.," Applied Optics **12**, 1202–1212 (1973).

[12] H. Ambar, Y. Aoki, N. Takai, and T. Asakura, "Mechanism of speckle reduction in laser-microscope images using a rotating optical fiber," Applied Physics B Photophysics and Laser Chemistry **38**, 71–78 (1985).

[13] H. Ambar, Y. Aoki, N. Takai, and T. Asakura, "Relationship of speckle size to the effectiveness of speckle reduction in laser microscope images using rotating optical fiber," Optik **74**, 22–26 (1986).

[14] B. Dingel and S. Kawata, "Speckle-free image in a laser-diode microscope by using the optical feedback effect," Optics Letters **18**, 549–551 (1993).

[15] M. Pircher, E. Gotzinger, R. Leitgeb, A. F. Fercher, and C. K. Hitzenberger, "Speckle reduction in optical coherence tomography by frequency compounding.," Journal of Biomedical Optics **8**, 565–569 (2003).

[16] D. C. Adler, T. H. Ko, and J. G. Fujimoto, "Speckle reduction in optical coherence tomography images by use of a spatially adaptive wavelet filter," Optics Letters **29**, 2878–2880 (2004).

[17] M. Bashkansky and J. Reintjes, "Statistics and reduction of speckle in optical coherence tomography," Optics Letters **25**, 545–547 (2000).

[18] J. M. Schmitt, S. H. Xiang, and K. M. Yung, "Speckle in optical coherence tomography.," Journal of Biomedical Optics **4**, 95–105 (1999).

[19] A. E. Desjardins, B. J. Vakoc, G. J. Tearney, and B. E. Bouma, "Speckle reduction in OCT using massively-parallel detection and frequency-domain ranging," Optics Express **14**, 4736–4745 (2006).

[20] K. V Chellappan, E. Erden, and H. Urey, "Laser-based displays: a review," Applied Optics **49**, F79–F98 (2010).

[21] T. Iwai and T. Asakura, "Speckle reduction in coherent information processing," Proceedings of the IEEE **84**, 765–781 (1996).

[22] R. S. Sirohi, ed., *Speckle Metrology* (Marcel Dekker, Inc., 1993).

[23] M.-A. Beeck and W. Hentschel, "Laser metrology - a diagnostic tool in automotive development processes," Optics and Lasers in Engineering **34**, 101–120 (2000).

[24] J. I. Amalvy, C. A. Lasquibar, R. Arizaga, H. Rabal, and M. Trivi, "Application of dynamic speckle interferometry to the drying of coatings," Progress in Organic Coatings **42**, 89–99 (2001).

[25] M. Muramatsu, G. H. Guedes, and N. G. Gaggioli, "Speckle correlation used to study the oxidation process in real time," Optics & Laser Technology **26**, 167–168 (1994).

[26] T. Fricke-Begemann, G. Gülker, K. D. Hinsch, and K. Wolff, "Corrosion monitoring with speckle correlation," Applied Optics **38**, 5948–5955 (1999).

[27] P. Zanetta and M. Facchini, "Local correlation of laser speckle applied to the study of salt efflorescence on stone surfaces," Optics Communications **104**, 35–38 (1993).

[28] B. B. Gorbatenko, V. P. Ryabukho, and L. A. Maksimova, "Reconstructing an object image using the laser speckle pattern of the diffraction field," Technical Physics Letters **30**, 741–743 (2004).

[29] B. B. Gorbatenko, L. A. Maksimova, N. Yu Mysina, and V. P. Ryabukho, "Technique of improvement of image reconstructing from registered intensity of diffraction speckle-fields," Computer Optics **36**, 46–50 (2012).

[30] T. W. Ng, "Optical distance sensing using digital speckle shearing interferometry," Optics and Lasers in Engineering **26**, 449–459 (1997).

[31] J. D. Briers, "Laser speckle contrast imaging for measuring blood flow," Optica Applicata **37**, 139–152 (2007).

[32] L. M. Veselov and I. A. Popov, "Statistical properties of modulated dynamic speckles," Optics and Spectroscopy **84**, 268–272 (1998).

[33] E. Nippolainen, D. V. Semenov, and A. A. Kamshilin, "Dynamic speckle effect induced by an acousto-optic deflector for fast range sensing.," Optics Letters **30**, 3147–3149 (2005).

[34] D. V. Semenov, E. Nippolainen, and A. A. Kamshilin, "Accuracy and resolution of a dynamic-speckle profilometer.," Applied Optics **45**, 411–418 (2006).

[35] D. V. Semenov, E. Nippolainen, and A. A. Kamshilin, "Comparison of acousto-optic deflectors for dynamic-speckle distance-measurement application," Journal of Optics A: Pure and Applied Optics **9**, 1–5 (2007).

[36] J. D. Rigden and E. I. Gordon, "The granularity of scattered optical maser light," Proceedings of the IRE **50**, 2367–2368 (1962).

[37] B. M. Oliver, "Sparkling spots and random diffraction," Proceedings of the IEEE **51**, 220–221 (1963).

[38] R. V. Langmuir, "Scattering of laser light," Applied Physics Letters **2**, 29–30 (1963).

[39] T. Asakura and N. Takai, "Dynamic laser speckles and their application to velocity measurements of the diffuse object," Applied physics **25**, 179–194 (1981).

[40] N. Takai, T. Iwai, and T. Asakura, "Correlation distance of dynamic speckles," Applied Optics **22**, 170–177 (1983).

[41] J. T. Ator, "Image-Velocity Sensing with Parallel-Slit Reticles," Journal of the Optical Society of America **53**, 1416 (1963).

[42] H. E. Meinema, "Film synchronizer for aerial cameras," Electronics **53**, 135–137 (1953).

[43] A. R. Gedance, "Comparison of infrared tracking systems," Journal of the Optical Society of America **51**, 1127–1130 (1961).

[44] J. T. Ator, "Image velocity sensing by optical correlation," Applied Optics **5**, 1325–1331 (1966).

[45] M. Gaster, "A new technique for the measurement of low fluid velocities," Journal of Fluid Mechanics **20**, 183–192 (1964).

[46] G. Stavis, "Optical diffraction velocimeter," Instruments and Control Systems **39**, 99–102 (1966).

[47] T. M. Sporton, "The scattering of coherent light from a rough surface," Journal of Physics D: Applied Physics **2**, 1027–1034 (1969).

[48] M. Giglio, S. Musazzi, and U. Perini, "Distance measurement from a moving object based on speckle velocity detection," Applied Optics **20**, 721–722 (1981).

[49] D. V. Semenov, E. Nippolainen, and A. A. Kamshilin, "Fast distance measurements by use of dynamic speckles," Optics Letters **30**, 248–250 (2005).

[50] I. Yamaguchi, "Speckle displacement and decorrelation in the diffraction and image fields for small object deformation," Optica Acta **28**, 1359–1376 (1981).

[51] M. Sjödahl, "Calculation of speckle displacement, decorrelation, and object-point location in imaging systems.," Applied Optics **34**, 7998–8010 (1995).

[52] P. Horváth, M. Hrabovsky, and P. Šmíd, "Full theory of speckle displacement and decorrelation in the image field by wave and geometrical descriptions and its application in mechanics," Journal of Modern Optics **51**, 725–742 (2004).

[53] M.-C. Amann, T. Bosch, M. Lescure, R. Myllyla, and M. Rioux, "Laser ranging: a critical review of usual techniques for distance measurement," Optical Engineering **40**, 10–19 (2001).

[54] T. Yoshimura, "Statistical properties of dynamic speckles," Journal of the Optical Society of America A **3**, 1032–1054 (1986).

[55] D. V. Semenov, S. V. Miridonov, E. Nippolainen, and A. A. Kamshilin, "Statistical properties of dynamic speckles formed by a deflecting laser beam," Optics Express **16**, 1238–1249 (2008).

[56] I. Yamaguchi and S. Komatsu, "Theory and applications of dynamic laser speckles due to in-plane object motion," Optica Acta **24**, 705–724 (1977).

[57] L. E. Estes, L. M. Narducci, and R. A. Tuft, "Scattering of Light from a Rotating Ground Glass," Journal of the Optical Society of America **61**, 1301–1306 (1971).

[58] S. Komatsu, I. Yamaguchi, and H. Saito, "Velocity measurement using structural change of speckle," Optics Communications **18**, 314–316 (1976).

[59] N. Takai, Sutanto, and T. Asakura, "Dynamic statistical properties of laser speckle due to longitudinal motion of a

diffuse object under Gaussian beam illumination," Journal of the Optical Society of America **70**, 827–834 (1980).

[60] N. Takai, T. Iwai, and T. Asakura, "Real-time velocity measurement for a diffuse object using zero-crossings of laser speckle," Journal of the Optical Society of America **70**, 450–455 (1980).

[61] M. Born and E. Wolf, *Principles of Optics* (Pergamon Press, 1959).

[62] B. Kedem, "Spectral analysis and discrimination by zero-crossings," Proceedings of the IEEE **74**, 1477–1493 (1986).

[63] V. Friedman, "A zero crossing algorithm for the estimation of the frequency of a single sinusoid in white noise," IEEE Transactions on Signal Processing **42**, 1565–1569 (1994).

[64] L. J. Griffiths, "Rapid measurement of digital instantaneous frequency," IEEE Transactions on Acoustics, Speech and Signal Processing **23**, 207–222 (1975).

[65] B. Boashash, "Estimating and interpreting the instantaneous frequency of a signal - part I: Fundamentals," Proceedings of the IEEE **80**, 520–538 (1992).

[66] B. Boashash, "Estimating and interpreting the instantaneous frequency of a signal - part II: Algorithms and applications," Proceedings of the IEEE **80**, 540–568 (1992).

[67] P. D. Welch, "The use of fast Fourier transform for the estimation of power spectra: a method based on time averaging over short, modified periodograms," IEEE Transactions on Audio and Electroacoustics **15**, 70–73 (1967).

[68] K. Barbé, R. Pintelon, and J. Schoukens, "Welch method revisited: nonparametric power spectrum estimation via circular overlap," IEEE Transactions on Signal Processing **58**, 553–565 (2010).

[69] J. B. Allen, "Short term spectral analysis, synthesis, and modification by discrete Fourier transform," IEEE Transactions on Acoustics, Speech and Signal Processing **25**, 235–238 (1977).

[70] J. B. Allen, "Applications of the short time Fourier transform to speech processing and spectral analysis," Proceedings of the IEEE ICASSP-82 1012–1015 (1982).

[71] J. B. Allen and L. R. Rabiner, "A unified approach to short-time Fourier analysis and synthesis," Proceedings of the IEEE **65**, 1558–1564 (1977).

[72] Y. Aizu and T. Asakura, *Spatial Filtering Velocimetry: Fundamentals and Applications* (Springer, 2006), Ch.4.

[73] T. Asaeda, K. Nousou, M. Imanisi, Y. Suzuki, and S. Katabami, "Inspection system and process," U.S. Patent 5,734,742 (March 31, 1998).

[74] V. R. Schneider and H.-J. Braach, "Method and device for the automatic detection of surface defects for continuously cast products with continuous mechanical removal of the material," U.S. Patent 6,184,924 (February 2, 2001).

[75] D. Rosenthal, S. Schulze, I. Schuster, P. Sudau, R. Fackert, A. Weinert, and W. Schumacher, "Method for detecting and classifying surface defects on continuously cast slabs," WO Patent 2,008,128,504 (October 31, 2008).

[76] C. Quan, S. H. Wang, C. J. Tay, H. M. Shang, and K. C. Chan, "Inspection of micro-cracks on solderball surface using a laser scattering method," Optics Communications **183**, 19–27 (2000).

[77] A. Abuazza, D. Brabazon, and M. A. El-Baradie, "Multi-beam fibre-optic laser scanning system for surface defect recognition," Journal of Materials Processing Technology **155-156**, 2065–2070 (2004).

[78] E. Matzan, "Dual laser web defect scanner," U.S. Patent 6,934,029 (August 23, 2005).

[79] Ø. Hjelle and M. Dæhlen, *Triangulations and Applications* (Springer, 2006).

[80] L. Wang, S. L. Jacques, and L. Zheng, "MCML--Monte Carlo modeling of light transport in multi-layered tissues," Computer Methods and Programs in Biomedicine **47**, 131–146 (1995).

[81] S. L. Jacques and L. Wang, "Monte Carlo modeling of light transport in tissues," in *Optical-Thermal Response of Laser-Irradiated Tissue*, A. J. Welch and M. J. C. van Gemert, eds. (Plenum, 1995), pp. 73–99.

[82] A. H. Hielscher, R. E. Alcouffe, and R. L. Barbour, "Comparison of finite-difference transport and diffusion calculations for photon migration in homogeneous and heterogeneous tissues," Physics in Medicine and Biology **43**, 1285–1302 (1998).

[83] R. A. J. Groenhuis, H. A. Ferwerda, and J. J. Ten Bosch, "Scattering and absorption of turbid materials determined from reflection measurements 1: Theory," Applied Optics **22**, 2456–2462 (1983).

[84] S. A. Carp, S. A. Prahl, and V. Venugopalan, "Radiative transport in the delta-P1 approximation: accuracy of fluence rate and optical penetration depth predictions in turbid semi-infinite media," Journal of Biomedical Optics **9**, 632–647 (2004).

[85] S. Xie, H. Li, and B. Li, "Measurement of optical penetration depth and refractive index of human tissue," Chinese Optics Letters **1**, 44–46 (2003).

[86] V. V. Tuchin, *Tissue Optics: Light Scattering Methods and Instruments for Medical Diagnosis* (SPIE Press, 2007).

[87] J. C. Dainty, ed., *Laser Speckle and Related Phenomena* (Springer-Verlag, 1984).

[88] T. K. Gaylord and M. G. Moharam, "Thin and thick gratings: terminology clarification," Applied Optics **20**, 3271–3273 (1981).

[89] M. P. Petrov, S. I. Stepanov, and A. V. Khomenko, *Photorefractive Crystals in Coherent Optical Systems* (Springer-Verlag, 1991).

[90] F. P. Bolin, L. E. Preuss, R. C. Taylor, and R. J. Ference, "Refractive index of some mammalian tissues using a fiber optic cladding method," Applied Optics **28**, 2297–2303 (1989).

Igor Sidorov

Applications of Dynamic Speckles in Optical Sensing

It would not be wrong to say that there is still potential for improvement of existing and development of completely new applications based on dynamic speckles, although they are known for many decades. In this thesis two novel methods based on dynamic speckles for detection of small defects of nontransparent surfaces and for estimation of light penetration depth in turbid media are presented. Also, theoretical limits of the measurement accuracy of the systems based on spatial filtering of dynamic speckles are examined. Besides, utilization of a micro-electro-mechanical system (MEMS) mirror as a deflector in the dynamic speckles range sensor is discussed in this work.

UNIVERSITY OF
EASTERN FINLAND

Publications of the University of Eastern Finland
Dissertations in Forestry and Natural Sciences

ISBN 978-952-61-1220-6